NASA-CR-169360
19820025547

A Reproduced Copy

OF

NASA CR- 169,360

Reproduced for NASA

by the

NASA Scientific and Technical Information Facility

FFNo 672 Aug 65

HOWARD UNIVERSITY
SCHOOL OF ENGINEERING
DEPARTMENT OF MECHANICAL ENGINEERING
WASHINGTON, D.C. 20059

FINAL REPORT

NASA GRANT: NSG-1414, Suppl. 4

THE DYNAMICS AND CONTROL OF LARGE
FLEXIBLE SPACE STRUCTURES-V

by

Peter M. Bainum
Professor of Aerospace Engineering
Principal Investigator

and

A.S.S.R. Reddy
R. Krishna
Cheick M. Diarra
V.K. Kumar
Graduate Research Assistants

August 1982

ABSTRACT

A general survey of the progress made in the current and past grant years in the areas of mathematical modelling of the system dynamics, structural analysis, development of control algorithms, and simulation of environmental disturbances is presented. The use of graph theory techniques is employed to examine the effects of inherent damping associated with LSST systems on the number and locations of the required control actuators. The presence of damping allows a greater flexibility to the selection of actuator locations under which the system is controllable, while the rank characteristics of the system matrix influence both the number and locations of the required actuators. A mathematical model of the forces and moments induced on a flexible orbiting beam due to solar radiation pressure is developed and typical steady-state open-loop responses obtained for the case when rotations and vibrations are limited to occur within the orbit plane. A preliminary controls analysis based on a truncated (13 mode) finite element model of the 122m. Hoop/Column antenna indicates that a minimum of six appropriately placed actuators is required for controllability. An algorithm to evaluate the coefficients which describe coupling between the rigid rotational and flexible modes and also intra-modal coupling has been developed and numerical evaluation based on the finite element model of Hoop/Column system is currently in progress.

ii

CONTENTS

LIST OF FIGURES

LIST OF FIGURES

LIST OF FIGURES

I. INTRODUCTION

The present grant represents a further extension of the effort initiated in previous grant years (May 1977 - May 1981) and reported in Refs. 1-7*. Techniques for controlling both the shape and orientation of very large inherently flexible proposed future spacecraft systems are being studied. Possible applications of such large structures in orbit include: large scale communications; earth observation and resource sensing systems; orbitally based electronic mail transmission; and as orbital platforms for the collection of solar energy and transmission (via microwave) to earth based receivers.

This report is subdivided into seven chapters. Chapter II is based on an invited general survey paper presented at the recent 10th IMACS World Congress on System Simulation and Scientific Computation, August 1982, and presents a general survey of the progress to date in four general areas: (1) mathematical modelling of the system dynamics; (2) structural analysis; (3) development of control algorithms, and (4) review of previous work in the simulation of environmental disturbances (mainly due to solar radiation pressure).

In Chapter III, the use of graph theoretic techniques, previously introduced[7] to simplify the eigenvalue calculation for LSST systems by reducing the system matrix to a collection of lower order sub-matrices,

---

*For references cited in this report, please see list of references at the end of each chapter.

is extended here to address the controllability of inherently damped large flexible space systems. A second paper to be presented at the 33rd International Astronautical Congress, Sept. 1982, forms the basis of this chapter.

At the operational altitudes of the future missions involving large space structures, the principal environmental disturbance is that due to solar radiation pressure. The effect of solar radiation (pressure) disturbance on a flexible orbiting free-free beam is addressed in Chapter IV, and to the authors' knowledge represents a first attempt to include such disturbances in the system dynamics of a flexible structure in orbit. (A paper based on Chapter IV has just been accepted for presentation at the 1983 AIAA Aerospace Sciences Meeting, January 1983.)

Our proposal[8] for the 1981-82 grant year originally emphasized work to be performed in three areas: (1) further analysis of environmental effects; (2) graph theory approach to the controllability, observability and eigenvalues of large scale systems; and (3) consideration of sensor and actuator dynamics. Shortly after submission of this document, we were advised by NASA-LRC that it was desired to redirect our effort so as to provide direct support to the synthesis of control laws for the LSST Hoop/Column Maypole Antenna system whose feasibility is currently being studied by the Harris Corporation, Melbourne, Flori . As a result of this the third task listed in our proposal was not considered, but, instead, Chapters V and VI represent our preliminary efforts in support of the Hoop/Column controls analysis.

In connection with this effort, the ORACLS computer algorithm[9], developed by NASA LRC is being used extensively in this effort. A "Versatile Hoop/ Column Antenna Structural Dynamics Model[10]" based on a NASTRAN finite element software package, prepared by the Harris Corporation, has been transmitted to us by NASA-LRC, togehter with a magnetic computer tape containing the eigenvectors for the first 34 modes of a single layer surface model of the 122m. model of the Hoop/Column – the latter received shortly before the end of the 1981-82 grant year. The effort described in Chapters V and VI is being continued during the 1982-83 grant year.

Chapter VII describes the main general conclusions together with recommendations for further work.

References - Introduction

1. Bainum, P.M. and Sellappan, R., "The Dynamics and Control of Large
   Flexible Space Structures," Final Report NASA Grant: NSG-1414,
   Part A: Discrete Model and Modal Control, Howard University, May 1978.

2. Bainum, Peter M., Kumar, V.K., and James, Paul K., "The Dynamics
   and Control of Large Flexible Space Structures," Final Report,
   NASA Grant: NSG-1414, Part B: Development of Continuum Model and
   Computer Simulation, Howard University, May 1978.

3. Bainum, P.M. and Reddy, A.S.S.R., "The Dynamics and Control of Large
   Space Structures II," Final Report, NASA Grant NSG-1414, Suppl. I,
   Part A: Shape and Orientation Control Using Point Actuators, Howard
   University, June 1979.

4. Bainum, P.M., James, P.K., Krishna, R., and Kumar, V.K., "The Dynamics
   and Control of Large Flexible Space Structures II" Final Report, NASA
   Grant NSG-1414, Suppl. 1, Part B: Model Development and Computer Simu-
   lation, Howard University, June 1979.

5. Bainum, P.M., Krishna, R., and James, P.K., "The Dynamics and Control
   of Large Flexible Space Structures III," Final Report, NASA Grant
   NSG-1414, Suppl. 2, Part A: Shape and Orientation Control of a
   Platform in Orbit using Point Actuators, Howard University, June 1980.

6. Bainum, P.M. and Kumar, V.K., "The Dynamics and Control of Large Flexible
   Space Structures III," Final Report, NASA Grant NSG-1414, Suppl. 2, Part B:
   The Modelling, Dynamics and Stability of Large Earth Pointing Orbiting
   Structures, Howard University, September 1980.

7. Bainum P.M., Kumar, V.K., Krishna, R. and Reddy, A.S.S.R. "The Dyanmics
   and Control of Large Flexible Space Structures IV," Final Report,
   NASA Grant NSG-1414, Suppl. 3, Howard University, August 1981.

8. Bainum, P.M., "Proposal for Research Grant on: The Dynamics and Control
   of Large Flexible Space Structures V ," Howard University (Submitted
   to NASA), Jan. 15, 1981.

9. Armstrong, E.S., "ORACLS - A System for Linear Quadratic-Gaussian
   Control Law Design," NASA Technical Paper 1106, April 1978.

10. "Versatile Hoop/Column Antenna Structural Dynamic Model," unpublished
    report, prepared by the Harris Corporation, 1982 (transmitted via
    NASA-LRC).

II. ON THE MODELLING AND SIMULATION OF THE DYNAMICS AND CONTROL OF LARGE FLEXIBLE ORBITING SYSTEMS

This paper attempts to review the steps involved in the development of mathematical models that can be used to simulate the in-orbit dynamics of large flexible systems. The use of graph theoretic techniques can often be used to reduce the computational effort involved for calculating the eigenvalues of large ordered systems. Computer generated graphical techniques may provide additional insight into the understanding of elastic modal shape functions of complex systems. Finally the numerical techniques commonly used to develop shape and attitude control laws will be briefly reviewed.

I. INTRODUCTION

Large, flexible orbiting systems have been proposed for possible use in communications, electronic orbital based mail systems, and in solar energy collection. The size and low weight to area ratio of such systems indicate that system flexibility is now the main consideration in the dynamics and control problem as compared to the inherently rigid nature of earlier spacecraft systems. For such large flexible systems both orientation and surface shape control will often be required.

Fig. 1 illustrates a conceptual plan of development of a system software capability for use in the analysis of the dynamics and control of large space structures technology (LSST) systems. This concept can be subdivided into four different stages: (1) system dynamics; (2) structural dynamics; (3) application of control algorithms; and (4) the simulation of the environmental disturbances. The most fundamental component is that of the modelling of the system dynamics of such systems in orbit.

II. MATHEMATICAL MODELLING OF SYSTEM DYNAMICS

Previously many authors analyzed spacecraft systems consisting of a primary rigid body and elastic appendages which represented solar panels, antenna booms, instrumentation platforms, etc. The hybrid coordinate modelling method as introduced by Meirovitch[1] and Nelson[1] and further developed by Likins[2] has been widely used in the study of such systems. The hybrid coordinates are comprised of the attitude (Euler) angles or quasi-coordinates of the primary body, as discrete coordinates, together with the displacement of the elastic appendages relative to the primary, characterized as distributed or modal coordinates.

The presence of rotors and movable damping mechanisms on the main part can be readily incorporated and the error involved in using a finite truncated series representation decreases with an increasing number of mode shapes. The remaining high frequency errors should be attenuated by suitable design of the closed-loop attitude control system.

When the size and weight to area ratio of such proposed future LSST systems indicates that the entire system must be considered to be flexible, the hybrid coordinate formulation may not always be readily adopted by simply assuming the mass and inertias of the (previously) rigid central part tend to zero in the limit. Santini[3] has developed a mathematical formulation for predicting the motion of a general orbiting flexible body using a continuum approach. Elastic deformations are considered small as compared with characteristic body dimensions. Equations are developed for both the rigid and elastic (generic) modes. This development is based on an a priori knowledge of the frequencies and modal shape functions of all modes to be included in the truncated system model. Kumar[4] and Bainum[4] have modified the development of Ref. 3 based on vector calculus so that elastic modal shape functions expressed in arbitrary systems of coordinates may be accommodated.

III. STRUCTURAL ANALYSIS

For simply isotropic structures, such as homogeneous beams and circular plates, closed form expressions are available for the elastic modal frequencies and shape functions. For more complex and/or nonisotropic systems numerical methods must be employed to obtain this information. Commonly used routines include versions of STRUDL and NASTRAN (the latter more complex algorithm may also be useful in the simulation of thermoelastic environmental effects). The use of computer generated graphics may also prove useful in understanding the elastic shape functions of complex systems when excited at different modal frequencies.

Fig. 2 illustrates the modal shape functions of a free-free circular elastic plate, showing the presence of the nodal lines and meridians as a function of the frequency parameter, λ.

For systems requiring a large number of elastic modes to accurately represent the system dynamics, graph theoretic techniques may provide an alternative to the numerical problems involved in calculating the eigenvalues (modal frequencies).[5] With this approach the system (stiffness) matrix can often be reduced to a system of lower ordered submatrices so that, under certain conditions, the eigenvalues of the original matrix are given by the union of the eigenvalues of the submatrices, including their multiplicity.[5] For large order systems this approach can substantially reduce the numerical effort involved with an improvement in accuracy. As an example, a free-free homogeneous square plate was considered in Ref. 5 where the original stiffness matrix contained a dimensionality of 16. Although this matrix was fairly sparse (less than 20% of the elements were non-zero), many of the non-zero elements were off-diagonal. Fig. 3 represents the digraph of the 16x16 stiffness matrix and indicates that, under appropriate conditions, the eigenvalues of the original matrix may be obtained by calculating the eigenvalues of seven sub-matrices; the largest dimensionality of any of the sub-matrices here is 4x4. Complete details describing this example and an algorithm that may be used to determine the sub-matrices, if the original matrix is reducible, are provided in Ref. 5. The non-zero elements of the stiffness matrix are given in Table I. The eigenvalues are evaluated from the original 16x16 stiffness matrix as well as the seven reduced order sub-matrices and are compared in Table II.

TABLE I

Non-zero elements of the K-matrix:

K(3,3)= 34.919	K(9,3)= 8.03522
K(12,4)= -19.9054	K(10,4)= 17.5471
K(14,6)= 15.4658	K(16,6)= 17.8584
K(15,7)= -11.6130	K(6,8)= 15.4658
K(16,8)= 96.9152	K(3,9)= 8.03522
K(4,10)= 17.5471	K(10,10)= 34.9190
K(9,11)= -5.31786	K(11,11)= 76.8770
K(12,12)= 326.604	K(7,13)= 17.5471
K(6,14)= 15.4658	K(8,14)= 56.1775
K(7,15)= -11.6130	K(13,15)= -19.9054
K(8,16)= 96.9152	K(14,16)= 96.9152
K(11,3)= -5.31786	K(4,4)= 265.337
K(6,6)= 13.3938	K(8,6)= 15.4658
K(7,7)= 34.9190	K(13,7)= 17.5471
K(8,8)= 386.913	K(14,8)= 56.1775
K(9,9)= 34.9190	K(11,9)= -5.31786
K(12,10)= -11.6130	K(3,11)= -5.31786
K(4,12)= -19.9054	K(10,12)= -11.6130
K(13,13)= 265.337	K(15,13)= -19.9054
K(14,14)= 386.913	K(16,14)= 96.9152
K(15,15)= 326.604	K(6,16)= 17.8584
K(16,16)= 1732.85	

TABLE II

Eigenvalues of the K matrix:

Submatrices		Original matrix
S_1	0.0	0.0
S_2	0.0	0.0
S_3	26.88378000	26.88378620
	41.36168802	41.36169439
	78.46953198	78.46953100
S_4	33.24206125	33.24206653
	260.2368175	260.2367428
	333.3811212	333.3811150
S_5	0.0	0.0
S_6	12.21269086	12.21269085
	330.7355000	330.7355804
	429.6358695	429.6359588
	1747.485740	1747.485839
S_7	33.24206125	33.24206653
	260.2368175	260.2367428
	333.3811212	333.3811150

The eigenvalues of the system are the eigenvalues of $M^{-1}K$ and as $M=I$, eigenvalues of $M^{-1}K=(1/m)$ times eigenvalues of K.

Before surface and orientation control systems can be designed, it is necessary to understand the dynamics and stability of the uncontrolled system. For large order systems an analytical approach to the stability problem is not feasible and numerical techniques must be employed to develop the system characteristic equation and the loci of its roots for different sets of system parameters.[6] As the number of modes retained in the truncated system model increases, expansion of the characteristic determinental equation becomes algebraically prohibitive. As an alternative an algorithm due to Leverrier[7,8] can be used to numerically determine the coefficients in the characteristic equation. In order to implement this algorithm the linearized equations must be written in standard state variable format.

IV. CONTROL ALGORITHMS

At this point the modelling of the control actuators can be added to the previously developed open-loop system models.[5,10] In general, an actuator placed at an arbitrary location on a large space structure will affect both the rigid and flexible modes. The location of such an actuator has definite implications on the system controllability. For large order systems the reachability matrix and term rank concepts, also developed from graph theoretic techniques, may be used to verify controllability and can be computationally more effective than numerical rank

tests of the system controllability matrix. The free-free square plate is again considered as an illustrative example in Ref. 5.

Three techniques are commonly used to develop control laws once the system controllability has been established. These include: (a) decoupling techniques; (b) pole placement (clustering); and (c) an application of the linear regulator problem from optimal control theory. These three techniques approach the controls problem from different points of view and each will be briefly discussed.

The decoupling technique can be applied in two distinct sub-cases: (1) where the linear state equations in the original coordinates are decoupled by using state variable feedback techniques; and (2) where the open loop linear equations are first transformed into a decoupled set in modal coordinates and then control laws are developed independently for each mode. It then becomes necessary to transform the control laws as expressed in modal coordinates to the actual control in the original coordinates.

As an example of sub-case (1), we assume that the linearized equations can be expressed as:

$$\bar{Z} = D\dot{Z} + EZ + BU \tag{1}$$

where $Z = (z_1, \ldots z_r, z_{r+1}, \ldots z_{r+n})^T$

describes the rigid body position displacements $(1,2 \ldots r)$ plus the n elastic (position.) coordinates retained in any truncated model. After selecting $U = K_r \dot{Z} + K_p Z$, we can rewrite the controlled motion equations as:

$$\ddot{Z} = (D + BK_r)\dot{Z} + (E + BK_p)Z \tag{2}$$

where K_r and K_p are evaluated such that $(D + BK_r)$ and $(E + BK_p)$ are diagonalized and thus yield the required damping and frequency of the controlled modes. The total number of rigid+elastic modes, $(r+n)$, must be equal to the number of actuators here to avoid the necessity of using pseudoinverse matrices.

For the second sub-case, as an example, let us consider a different form of Eq. (1) in terms of the mass (M) and stiffness (K) matrices, where $D=0$.

$$M \ddot{Z} + KZ = F = BU \tag{3}$$

With the following type of transformation: $Z = \phi q$, Eq. (3) may be recast in terms of the modal coordinates, q, and the transformation matrix (involving the eigenvectors), ϕ, as:

$$[\phi^T M \phi]\ddot{q} + [\phi^T K \phi]q = \phi^T F \tag{4}$$

such that $\phi^T M \phi$ and $\phi^T K \phi$ are diagonalized

$$[^\cdot M_i^\cdot] \ddot{q} + [^\cdot K_i^\cdot]q = \phi^T F = F' \tag{5}$$

It is then possible to design the control laws, F', in the modal space so that independent control of each of the modes can be achieved. A transformation is then required to obtain the control laws in the original coordinates, F, and, then, for a given location of actuators, the actual control from: $U = B^{-1}F = B^{-1}(\phi^T)^{-1}F'$.

In the pole clustering method the overall transient requirements of the system are considered instead of concentrating on the behavior of the individual coordinates. The linearized system equations, Eq. (1), can be recast in the state space format as:

$$\dot{X} = AX + BU \tag{6}$$

where

$$X = [z_1 \ldots z_r, z_{r+1} \ldots z_{r+n}, \dot{z}_1 \ldots \dot{z}_r, \dot{z}_{r+1} \ldots \dot{z}_{r+n}]^T$$

The control, $U = -KX$, is then selected by using a digital computer algorithm such as ORACLS[11] such that $(A-BK)$ has the identical negative real part in each of its eigenvalues. Although the number of actuators can be less than the number of modes, a limitation of this particular algorithm is that the gains are selected such that all of the closed-loop poles lie on a line parallel to the imaginary axis. The algorithm is useful, however, when it is important that each mode in the system satisfy some minimum damping characteristics.

The linear regulator theory allows the analyst to set, a priori, distinct penalty weighting functions on the control effort as well as the state variables. The control law, $U = -KX$, is selected such that the following performance index is minimized

$$J = \int_o^\infty (X^T QX + U^T RU)dt \tag{7}$$

where Q and R are positive definite penalty matrices. The steady state solution of the matrix Riccati equation of dimension equal to the state has to be solved in order to obtain the gain matrices, K (which represent the positive definite solution to the algebraic matrix Riccati equations).

A computer algorithm within the CRACLS[11] software package can be used to obtain the gain matrices, K, for different combinations of the Q and R penalty matrices. This algorithm utilizes the Newton-Raphson method of solving the Riccati equation.

Both the linear regulator problem and the pole clustering methods can result in some of the closed loop frequencies being orders of magnitude greater than those of the uncontrolled system. These higher frequencies may also correspond to the frequencies of higher modes not included in the previously truncated system model. In order to completely consider such effects the order of the original system model would have to be increased in order to

avoid the effects of control spillover. On the other hand, these methods have the advantage that they car be applied to situations where the number of actuators is less than the number of modes in the mathematical model, in contrast to the usual applications of the decoupling methods. Examples of the application of the various control algorithms are given in Ref. 10. As an example, a typical application of decoupling, using state variable feedback for the orientation and shape control of a a free-free square plate nominally following the local vertical with its larger surface normal to the orbit normal is considered. The model contains three rigid rotational modes and the first three transverse flexible modes, with six actuators assumed to be located as shown in Fig. 4. The decoupling gains are selected in order to produce 20% of critical damping in each of the rigid modes and the fundamental elastic mode and 10% of critical damping in the second and third flexible modes. The controlled state response is given in Fig. 5 and the corresponding time history of the required control forces is illustrated in Fig. 6.

V. SIMULATION OF ENVIRONMENTAL DISTURBANCES

The principal disturbance forces and torques acting on a large flexible system in orbit are the gyroscopic and gravity-gradient torques associated with the orbital motion, the control torques, and those torques due to the environment. In the formulation of Refs. 3 and 4 the gyroscopic and gravity-gradient torques are included in the model of the system dynamics. If other formulations are employed, such as general finite element methods, which do not account for the orbital dynamics, the effects of the gyroscopic and gravity-gradient torques should be carefully considered before deleting them from the dynamic model. The treatment of control modelling and algorithms was examined in the last section of this paper and no further elaboration will be provided here.

Environmental disturbances can be attributed mainly to the effects of solar radiation pressure, except in very low earth orbit where the aerodynamic drag forces predominate. Moments due to solar radiation pressure are induced if the center of solar radiation pressure is not co-located with the system center of mass. The location of the center of pressure is dependent on the surface characteristics as well as the geometrical shape of the structure. In addition, due to solar heating, thermal gradients can be induced in the structure which may result in appreciable thermal strains. As a result, the structure will undergo deformations which will further contribute to the forces and torques caused by the solar pressure.

Several investigators have considered the effect of solar radiation pressure on the dynamics of spacecraft. The majority of the spacecraft modelled consisted of a smaller rigid

central satellite to which flat plate appendages, also treated as rigid, were assumed to be attached. A few authors showed how the solar pressure moments generated could be used for satellite attitude control by controlling the orientation of plates and/or vanes which could rotate at the ends of the appendages[2,13] An extension of these models to include large inherently flexible orbiting systems is needed before the nature of the environmental disturbances on proposed LSST systems can be completely understood.

VI. CONCLUDING COMMENTS

This paper has attempted to review the key steps required for the modelling and simulation of the dynamics and control of future proposed large flexible orbiting systems which will require, in general, both shape as well as orientation (attitude) control. Problem areas, mainly associated with the large order of such system models, are highlighted. The widespread use of various computer algorithms required at different stages of the analysis should be noted.

References

1. Meirovitch, L. and Nelson, H.D., High-Spin Motion of a Satellite Containing Elastic Parts, Journal of Spacecraft and Rockets, Vol. 13, (1976), 1597-1602.

2. Likins, P.W., Dynamics and Control of Flexible Space Vehicles, Jet Propulsion Laboratory, Pasadena, Calif., TR32-1329, 1969.

3. Santini, P., Stability of Flexible Spacecrafts, Acta Astronautica, Vol. 3, (1977), 685-713.

4. Kumar, V.K. and Bainum, P.M., Dynamics of a Flexible Body in Orbit, AIAA/AAS Astrodynamics Conference, Palo Alto, Calif., August 7-9, 1978, Paper No. 78-1418; also, Journal of Guidance and Control, Vol. 3, (1980), 90-02.

5. Reddy, A.S.S.R. and Bainum, P.M., Graph Theory Approach to the Eigenvalue Problem of Large Space Structures, Third VPI&SU/AIAA Symposium on Dynamics and Control of Large Flexible Spacecraft, Blacksburg, Va., June 15-17, 1981.

6. Bainum, P.M. and Kumar, V.K., On the Dynamics of Large Orbiting Flexible Beams and Platforms Oriented along the Local Horizontal, 31st International Astronautical Congress, Tokyo, Japan, Sept. 21-28, 1980, Paper No. IAF 80 E-230; also, to appear, Acta Astronautica.

7. Zadeh, L.A., and Desoer, C.A., Linear System Theory, (McGraw Hill Book Co., New York 1963), 303-305.

8. Malsa, J.L., and Jonas, S.K., Computer
   Programs for Computational Assistance in
   the Study of Linear Control Theory, (McGraw
   Hill Book Co., New York, 1970), 6-11.

9. Bainua, P.M. and Reddy, A.S.S.R., On the
   Controllability of a Long Flexible Beam in
   Orbit, Proceedings of the Second AIAA Sym-
   posium on Dynamics and Control of Large
   Flexible Spacecraft, June 21-23, 1979, (VPI&
   SU Press, Ed. L. Mairovitch, 1980), 145-
   159.

1 10. Reddy, A.S.S.R., Bainum, P.M., Hamer, H.A.,
   and Krishna, R., Control of a Large Flexible
   Platform in Orbit, AIAA/AAS Astrodynamics
   Conference, Danvers, Mass., Aug. 11-13,
   1980, Paper No. 80-1668; also, Journal of
   Guidance and Control, Vol. 4, (1981), 642-
   648.

11. Armstrong, E.S., ORACLS - A System for
    Linear-Quadratic-Gaussian Control Law De-
    sign, NASA Technical Paper 1106, April
    1978.

12. Modi, V.J. and Panda, K.C., Solar Pressure
    Control of a Dual Spin Satellite, Journal
    of Spacecraft and Rockets, Vol. 10, (1973),
    355-351.

13. Pande, K.C., Davis, M.S., and Modi, V.J.,
    Time Optimal Pitch Control of Satellites
    using Solar Radiation Pressure, Journal
    of Spacecraft and Rockets, Vol. 11, (1974),
    601-603.

```
┌─────────────────────────┐         ┌─────────────────────────┐
│ SYSTEM DYNAMICS         │         │ STRUCTURAL ANALYSIS     │
├─────────────────────────┤         ├─────────────────────────┤
│ nonlinear d.e. –        │         │ √STRUDL-II              │
│ LSST                    │         │                         │
│                         │         │  det. frequencies       │
│ √beam – 2-D             │◄────────│  mode shapes            │
│ √plate 3-D;             │         │                         │
│                         │         │  NASTRAN                │
│ √shallow. spherical     │         │                         │
│  shell – 3-D            │         └─────────────────────────┘
│                         │
│ Hoop/Column (IP)        │
└─────────────────────────┘

┌─────────────────────────┐         ┌─────────────────────────┐
│ CONTROL ALGORITHMS      │         │ ENVIRONMENTAL           │
├─────────────────────────┤         ├─────────────────────────┤
│ √Jones & Melsa –        │         │ (IP) Solar              │
│  opt. control           │         │       Radiation         │
│                         │         │       Forces/Torques    │
│ √ORACLS – opt.          │         │                         │
│            control      │         │ (IP) Thermal Effects    │
│            decoupl-      │        └─────────────────────────┘
│            ing          │
│            pole         │
│            place-       │
│            ment         │
│                         │
│ (IP) Hybrid systems-    │
│      passive/active     │
└─────────────────────────┘
```
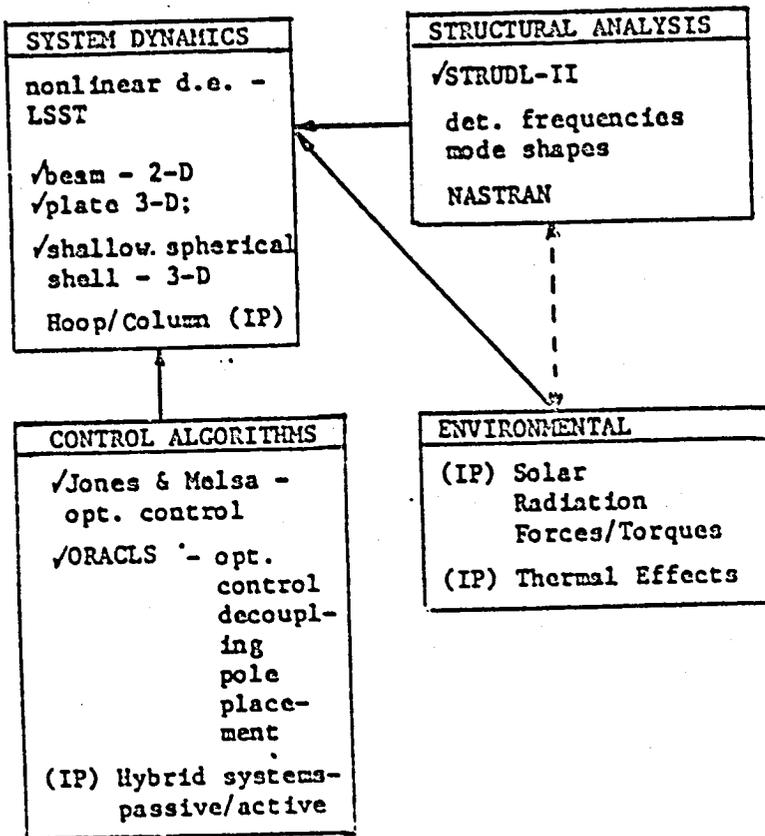
√operational
IP- in progress

Fig. 1   Development of system software for LSST
         dynamics analysis

j=0, p=2, λ^2=5.253

j=1, p=0, λ^2=9.084

j=1, p=1, λ^2=20.52

j=2, p=0, λ^2=38.55

----- nodal lines

λ = frequency parameter

j = number of nodal circles

p = number of nodal meridians

j=2, p=1, λ^2=59.86
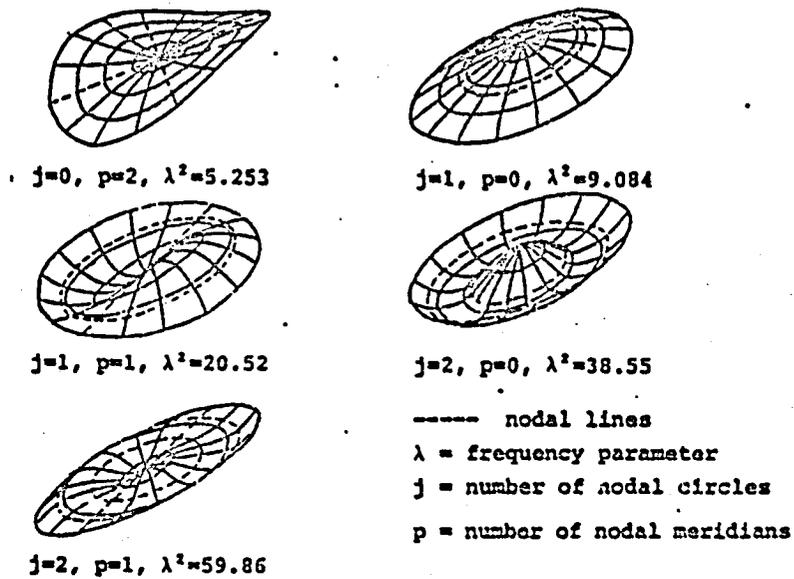
Fig. 2 Mode shapes of a free-free circular plate (computer generated at Howard University).

1   2   3   9   11   4   10   12   5   6   8   14   16   7   13   15
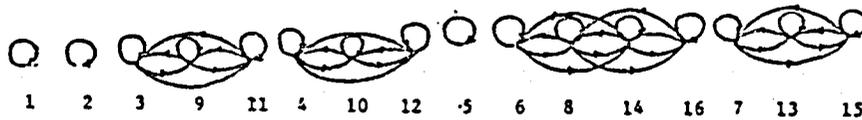
Fig. 3 Digraph of 16x16 K matrix.

2.7
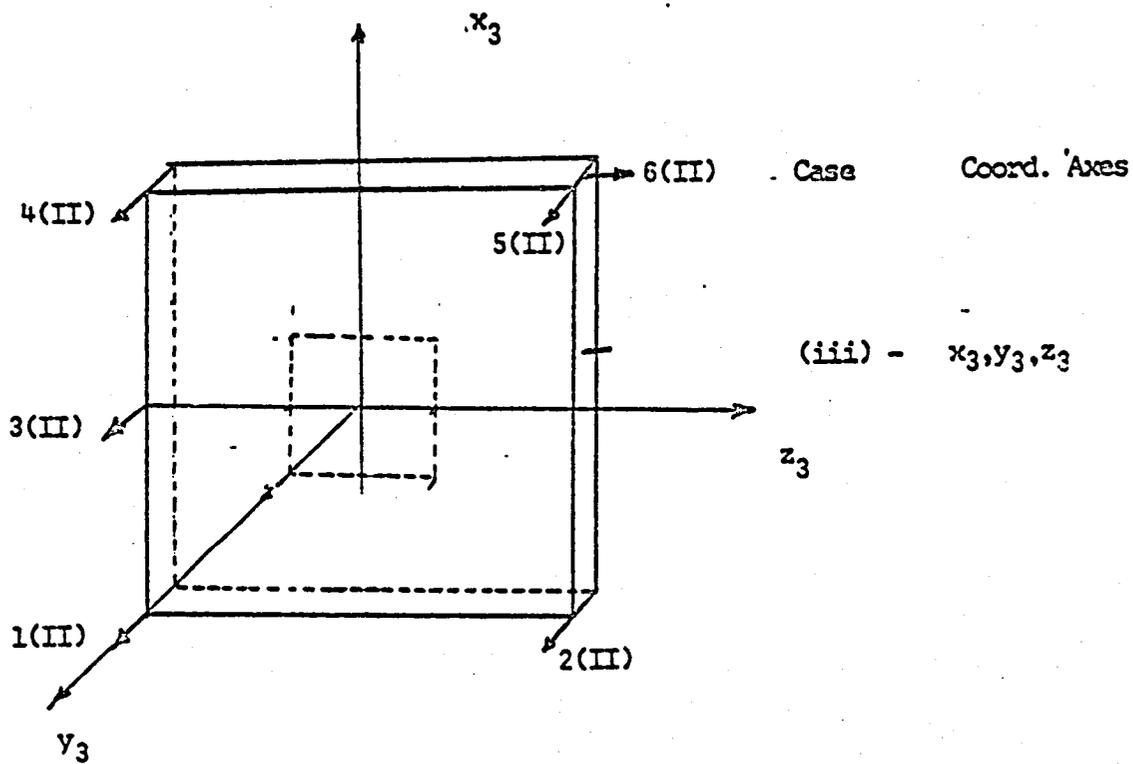
Fig. 4 Location of set of actuators (II).
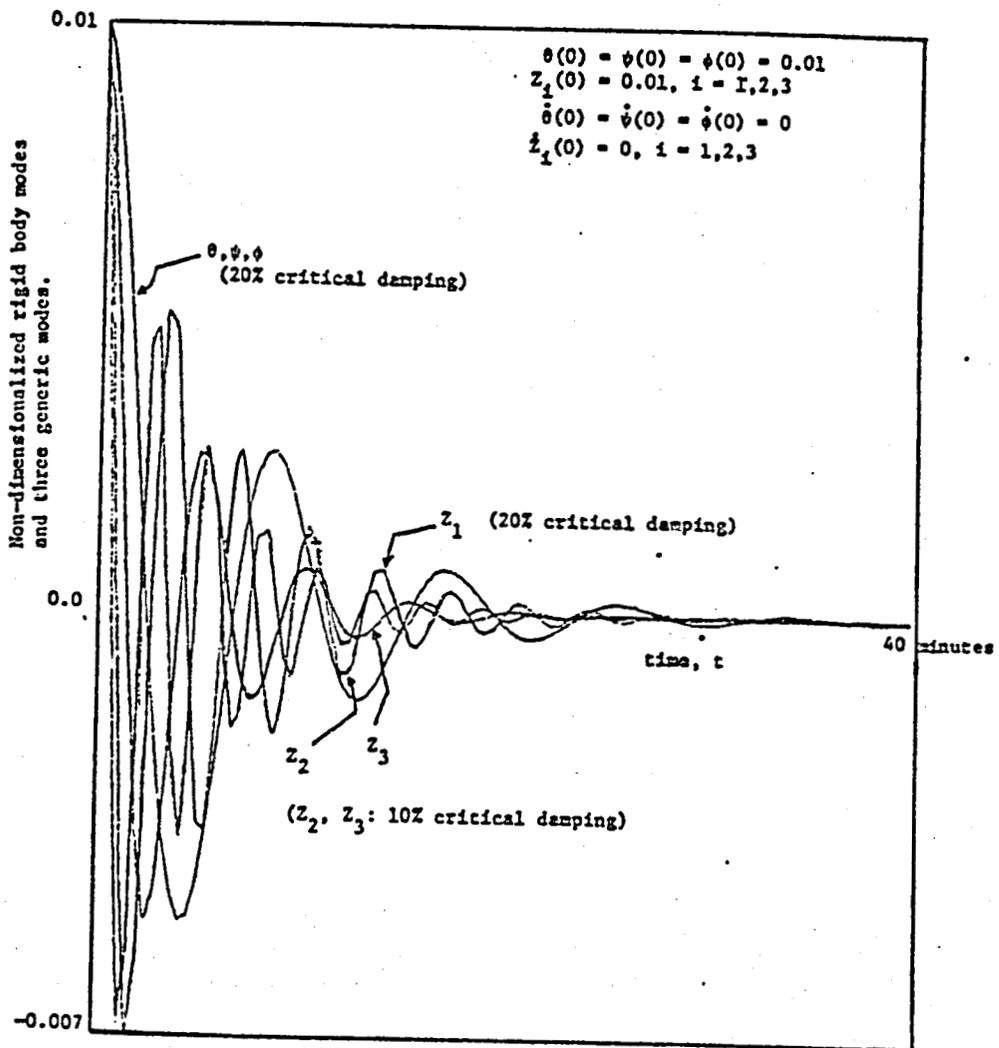
Fig. 5 Controlled state response for all combinations of orientations and actuator locations.

2.9
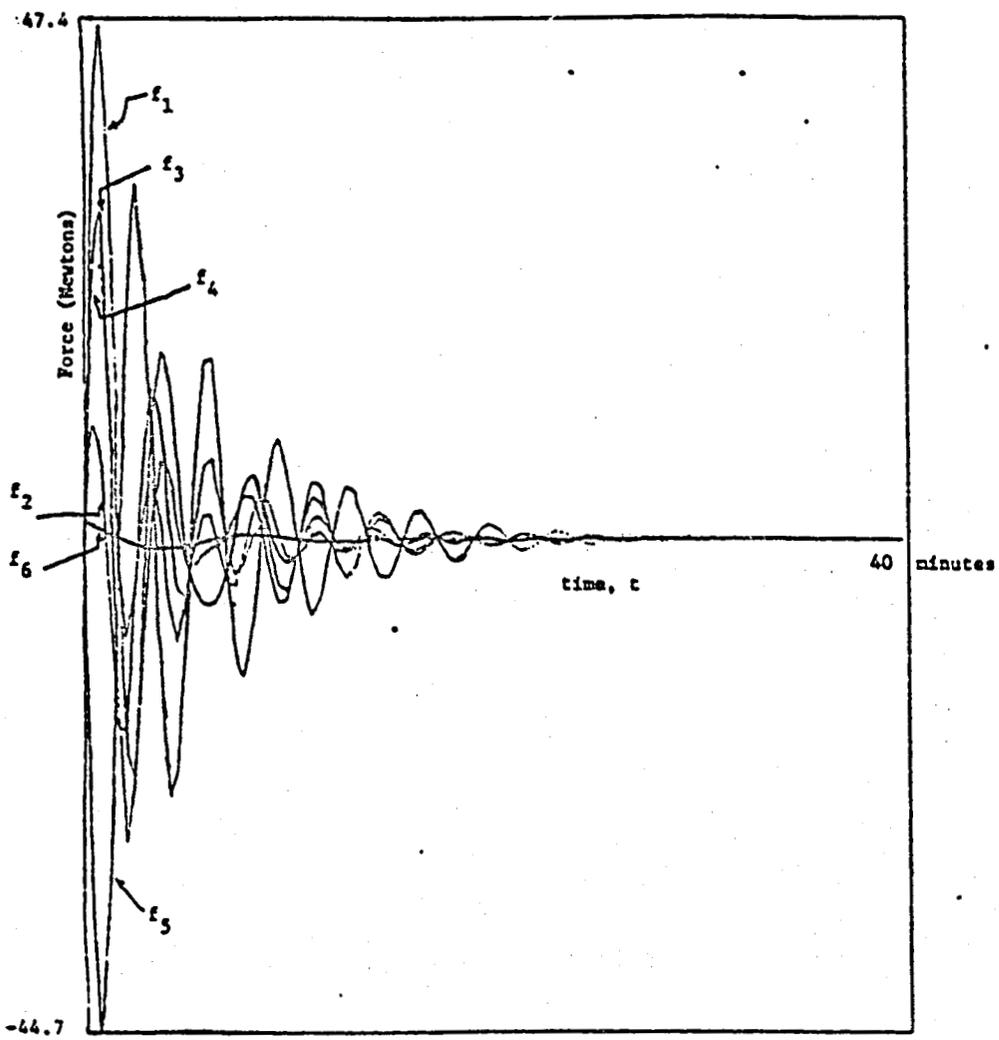
Fig. 6 Control force time history for Case (iii)-II.

2.10

III. CONTROLLABILITY OF INHERENTLY DAMPED LARGE FLEXIBLE SPACE STRUCTURES

Abstract

·Graph theoretic techniques are used to study controllability of linear systems which could represent large flexible orbiting space systems with inherent damping. The controllability of the pair of matrices representing the system state and control influence matrices is assured when all states in the model are reachable in a digraph sense from at least one input and also when the term rank of a Boolean matrix whose non trivial components are based on the state and control influence matrices has a term rank of the order of the state vector. It is seen that the damping matrix does not influence the required number of actuators but gives flexibility to the possible locations of the actuators for which the system is controllable, and that the stiffness matrix term rank deficiency dictates the number as well as the location of the required actuators. Specific examples include a model of a shallow spherical orbiting shell where both orientation and shape control are required, and also a smaller dimensional numerical example (unrelated to the shell) which readily demonstrates the effect of damping.

Nomenclature

A	$n \times n$ system matrix
$\bar{A}$	$2n \times 2n$ system matrix
B, B_p	$n \times m$ control influence matrices
$\bar{B}$	$2n \times m$ control influence matrix
D	$n \times n$ damping matrix
D'	$n \times n$ modified damping matrix
A_B, B_B, D_B'	Boolean equivalents of A, B and D' matrices
K	$n \times n$ stiffness matrix
M	$n \times n$ mass matrix
R	reachability matrix
R'	$n \times m$ submatrix of matrix R
S	diagonal matrix $(r \times r)$
U	$m \times 1$ input vector
V_1	$n \times n$ unitary orthogonal matrix
V_2	$m \times m$ unitary orthogonal matrix
x	$n \times 1$ vector
Σ	$n \times m$ matrix
u	small parameter
σ_i	$\underline{i^{th}}$ singular value of matrix A

I. Introduction

Any linear, time invariant dynamical system can be, in general represented by:

$$\dot{X} = AX + BU \tag{1}$$

where

X is an $n \times 1$ state vector of the system
A is an $n \times n$ system state matrix
B is an $n \times m$ control influence matrix
U is an $m \times 1$ input of the system.

The system described by equation (1) is said to be controllable if, with finite U and in finite time, the system (1) can be transferred from any state to any other state. This concept was first introduced by Richard E. Kalman.[1] The verification of controllability is essential for control system design as no control law should be designed for a system which is not controllable. The controllability concept is even more important for large space structural systems whose dimensionality is very large. If the design of the control system is undertaken without first verifying controllability, a considerable amount of effort may be wasted, through the failure to arrive at any satisfactory control law for an uncontrollable system.

In the following sections, the concept of controllability, as a property of the A and B matrices, is reviewed.

The system, (1) is controllable if and only if[1,2]:

$$\text{rank } (B, AB, A^2B, \ldots, A^{n-1}B) = n \tag{2}$$
$$\text{or} \quad \text{rank } (B, A - \lambda_i I) = n, \; i = 1, 2, \ldots n \tag{3}$$

where λ_i are the eigenvalues of the matrix, A.

The determination of the rank of the matrix in equation (2) poses the problem of selecting n independent columns out of nm columns and this could be done by such numerical techniques as the singular value decomposition of a matrix.[3]

The singular value decomposition is a numerical algorithm used to find the numerical rank of a rectangular matrix, A, (n×m, say n>m) through the evaluation of two orthogonal (unitary) matrices, V_1 and V_2 such that

$$A = V_1 \Sigma V_2^T \tag{4}$$

where

$$\Sigma = \begin{bmatrix} S & 0 \\ 0 & 0 \end{bmatrix} = V_1^T A V_2 \tag{5}$$

and $S = \text{diag } (\sigma_1, \sigma_2, \ldots, \sigma_r)$

with $\sigma_1 \geq \sigma_2 \geq \ldots > \sigma_r > 0$, being singular values of A. The $\sigma_1, \sigma_2, \ldots, \sigma_r$ are the non zero eigenvalues of the matrix AA^T (or A^TA) and r is the rank of the matrix A. The technique of finding the singular values of A by evaluating the eigenvalues of AA^T or A^TA is, in general, less accurate than using singular value decomposition techniques and may result in erroneous conclusions, as is demonstrated by the following example.[3]

Let
$$A = \begin{bmatrix} 1 & 1 \\ \mu & 0 \\ 0 & \mu \end{bmatrix} \qquad (6)$$

Then [if $1+\mu^2=1$, but $1+\mu\neq1$, for the computer accuracy involved]

$$A^TA = \begin{bmatrix} 1 & 1 \\ 1 & 1 \end{bmatrix} \qquad (7)$$

The eigenvalues of this approximation to A^TA are $\sqrt{2}$ and 0, respectively, whereas the precise eigenvalues of A^TA are found to be $\sqrt{2+\mu^2}$ and μ, respectively.

The use of the singular value decomposition technique, itself, may result in numerical problems when the magnitude of the largest singular value of the matrix A, is an order of magnitude (or more) different from that of the smallest singular value. [A complete discussion of the singular value decomposition technique is given in Ref. 3. It should be noted that with the use of this algorithm, it is unnecessary to directly evaluate the singular values of the A matrix. The rank determination is accomplished based on the unitary, orthogonal properties of the matrices V_1 and V_2 within the algorithm.]

The application of the controllability condition in equation (3) requires the determination of the eigenvalues of the matrix A and the evaluation of the rank of a matrix of order $[nx(n+m)]$ for each of the n eigenvalues. This scheme is more attractive than that of condition (2) as the problem of rank evaluation of an nxnm matrix is reduced to the rank evaluations of n matrices each of dimension $[nx(n+m)]$. The eigenvalues are, in general, needed for the structural dynamic analysis of the system and may, thus, be already available for this phase of the control system design.

II. Controllability of Large Space Structures

The dynamical equations of a large space structure system are, in general, described by a set of linear second order coupled differential equations as:

$$M\ddot{X} + D\dot{X} + KX = B_p U \qquad (8)$$

where
- X is the nx1 vector of the generalized coordinates
- M is the mass matrix (nxn)
- D is the damping matrix (nxn) (can include viscous damping as well as gyroscopic effects)

- K is the stiffness matrix
- B_p is the control influence matrix
- U is the mx1 vector of inputs.

The dynamical system of equations (8) can be rewritten as a set of first order differential equations (in standard state space form as):

$$\begin{bmatrix} \dot{X} \\ \ddot{X} \end{bmatrix} = \begin{bmatrix} 0 & I \\ \hline -M^{-1}K & -M^{-1}D \end{bmatrix} \begin{bmatrix} X \\ \dot{X} \end{bmatrix} + \begin{bmatrix} 0 \\ M^{-1}B_p \end{bmatrix} U \qquad (9)$$

Equation (9) can be considered as

$$\dot{\bar{X}} = \bar{A}\bar{X} + \bar{B}U \qquad (10)$$

where
$$\bar{X} = [X, \dot{X}]^T$$

$$\bar{A} = \begin{bmatrix} 0 & I \\ \hline A & D' \end{bmatrix} \qquad \bar{B} = \begin{bmatrix} 0 \\ B \end{bmatrix} \qquad (11)$$

and $A = -M^{-1}K$, $D' = -M^{-1}D$, $B = M^{-1}B_p$.

The controllability condition (2) for this system can be written as:

$$\text{rank} \ [\bar{B}, \bar{A}\bar{B}, \ldots, \bar{A}^{2n-1}\bar{B}] = 2n \qquad (12)$$

If we assume D=0, which is true for many idealized free vibrating structures, the controllability matrix[4]

$$C = [\bar{B}, \bar{A}\bar{B}, \ldots, \bar{A}^{2n-1}\bar{B}], \qquad (13)$$

becomes

$$C = \begin{bmatrix} 0 & B & 0 & AB \\ B & 0 & AB & 0 \end{bmatrix} \cdots \begin{bmatrix} A^{n-1}B \\ 0 \end{bmatrix} \qquad (14)$$

It can be very easily seen that C has a rank 2n if and only if

$$\text{rank} \ [B, AB, \ldots, A^{n-1}B] = n \qquad (15)$$

which leads to the following theorem[4]:

Theorem:
The pair $\begin{bmatrix} 0 & I \\ \hline A & 0 \end{bmatrix}$, $\begin{bmatrix} 0 \\ B \end{bmatrix}$ is controllable if and only if the pair [A,B] is controllable.

This theorem reduces the determination of the controllability of a 2nth order system to the determination of the controllability of an equivalent nth order system. In general for large space structure applications, n itself may still be sufficiently large and, thus, numerical techniques would be required in order to determine controllability. This theorem is based on the inherent assumption that D=0 and no insight can be drawn when D is not equal to zero. The effect of the matrix, D, on controllability is studied in this paper using the graph theoretic definition of controllability.

III. Graph Theoretic Definition of Controllability

Given the general, linear, time invariant dynamical system described by equation (1), repeated here as:

$$X = AX + BU \tag{16}$$

the pair [A,B] is controllable if and only if:

(1) the term rank of $\begin{bmatrix} A_B & B_B \\ 0 & 0 \end{bmatrix} = n$

where A_B, B_B are the Boolean equivalents of the matrices A and B, respectively; and
(2) all states in the system are reachable from at least one input in the digraph sense.

The two terms, term rank and reachability, are explained here.

Term rank is the maximum rank a matrix can achieve due to the locations of the non zero, non fixed elements of the matrix rather than due to the numerical values of the elements. A complete discussion of this concept is provided in the Appendix.

Reachability. If one draws a digraph for the extended square matrix $\begin{bmatrix} A & B \\ 0 & 0 \end{bmatrix}$ and finds the input-state reachability matrix as explained in the Appendix, there must be at least one non zero entry for every row of the submatrix (R') in the reachability matrix, R, formed from the row and column indices 1 to n, and n+1 to n+m, respectively, as shown in equation (17) where n is the number of states in the system and m is the number of actuators.

$$R = \tag{17}$$

IV. Controllability of Systems with Inherent Damping

The dynamics of large space systems with inherent damping can be written as (repeating equation (9) with the notation defined in equation (10))

$$\begin{bmatrix} \dot{x} \\ \ddot{x} \end{bmatrix} = \begin{bmatrix} 0 & I \\ A & D' \end{bmatrix} \begin{bmatrix} x \\ \dot{x} \end{bmatrix} + \begin{bmatrix} 0 \\ B \end{bmatrix} U \tag{18}$$

The digraph for the system matrices $\overline{A}$, $\overline{B}$ can be drawn in general as shown in Fig. 1.

The elements of $\overline{A}(i,i+n)$, $i=1,2,\ldots,n$ -i.e. those elements of A appearing in the identity matrix - are represented in the digraph by the (solid) lines joining the nodes (i+n) to i where $i=1,2,\ldots,n$. The elements of $\overline{A}(i+n,j)$, $i=1,2,\ldots,n$, $j=1,2,\ldots,n$ i.e. those elements of A appearing in A are represented in the digraph by the (dashed) lines joining the jth node to the (i+n)th node. The elements of $\overline{A}(i+n,j+n)$, $i=1,2,\ldots,n$, $j=1,2,\ldots,n$ i.e. those elements of A appearing in D' are represented in the digraph by the (dotted) lines connecting the (j+n)th node to the (i+n)th node.

The elements of B [the lower half of $\overline{B} = \overline{B}(i+n,j)$], $B_p(i,j)$, $i=1,2,\ldots,n$, $j=1,2,\ldots,m$, are represented in the digraph by the (double solid) lines joining the jth actuator [the (2n+j)th node, here] to the (i+n)th node.

From the reachability condition, it is observed that the lines in the digraph due to the D matrix can supplement those lines due to the B_p matrix. For example suppose that due to the structure of D, there is a directed (dotted) line from node (n+3) to node (n+2) in Fig. 1. Suppose that the mth actuator represented by node (2n+m) can directly influence node (n+3). Then it is clear the actuators number 2 and 3 (represented by node 2n+2 and 2n+3, respectively) need not be present in order to influence nodes n+2 and n+3. Thus the damping matrix can allow a greater flexibility in this selection of the actuator locations. Although based on this argument one could construe that the D matrix influences the number of actuators (that could be removed), it should be remembered that the minimum number of actuators required is dictated from the term rank condition which will now be discussed.

For the system represented by equation (18) to be controllable, the term rank (as explained in the Appendix) of the Boolean matrix, a

$$\begin{bmatrix} 0 & I & 0 \\ A_B & D'_B & B_B \\ 0 & 0 & 0 \end{bmatrix} = n \tag{19}$$

must be 2n. Note that the dimensionality of the state vector in equation (18) is 2n. If A has term rank less than n, then the term rank of the (2n+m)th order Boolean matrix in equation (19) can only be augmented due to the presence of B_B, since the Det $[A_B] = -$ Det $[A_B]$. Thus, D_B can not be used to augment the term rank of the Boolean equivalent of the state matrix A in equation (18).

In summary, the damping matrix, D, has an effect on the location of the actuators, while the matrix A has an impact on the location as well as the number of actuators.

V. Numerical Examples

The use of graph theoretic techniques in the determination of controllability and the amount of information about the location of the actuators and the number of actuators needed is demonstrated using the model of an orbiting shallow spherical shell in orbit with and without the stabilizing dumbbell (Fig 2).[6]

The Boolean Equivalent of the system matrix (A)[7] for a shallow spherical shell is given in Fig. 3. The digraph is given in Fig. 4. From the digraph it can be seen that the nodes may be subgrouped as:

$$\begin{vmatrix} 10 & 11 & 12 & 13 & 14 & 15 & 16 & 17 & 18 \\ 1 & 2 & 3 & 4 & 5 & 6 & 7 & 8 & 9 \end{vmatrix}$$

To reach all the 18 states from at least one input, control actuators must directly influence the following nodes: (a) (10 or 11); (b) at least one of the nodes (12-15); (c) (16); (d) (17); and (e) (18). The system matrix, A, has a term rank deficiency of 1 (note the presence of only zeros in the first column, Fig. 3) and, thus, one actuator is required for controllability. This actuator must be placed such that the above mentioned states are directly influenced.

The model of a shallow spherical shell with a stabilizing dumbbell[6,7] is considered as another example for controllability considerations. The Boolean equivalent of the 22nd ordered system matrix A is given in Fig. 5 and the digraph is shown in Fig. 6. From the digraph it can be seen that the total states can be subdivided into two groups

$$\begin{vmatrix} 12 & 16 & 17 & 18 & 19 & 20 & 21 & 22 & 13 & 14 & 15 \\ 1 & 5 & 6 & 7 & 8 & 9 & 10 & 11 & 2 & 3 & 4 \end{vmatrix}$$

The control actuators must directly influence one or more states from group (1) and one or more states from group (2). The system matrix here has full term rank and, thus, one actuator is sufficient to establish controllability.

The two practical examples considered in this section to this point do not specifically illustrate the independence between the number of actuators required and the damping matrix. To illustrate this effect an example of sixth order is created and analyzed.

It is assumed that the system matrix is given by

$$\bar{A} = \begin{bmatrix} 0 & 0 & 0 & 1 & 0 & 0 \\ 0 & 0 & 0 & 0 & 1 & 0 \\ 0 & 0 & 0 & 0 & 0 & 1 \\ 1 & 0 & 0 & 1.0 & 2.0 & 3.0 \\ 0 & 0 & 0 & -10.0 & 5.0 & 6.0 \\ 0 & 0 & 0 & 7.0 & 8.0 & 9.0 \end{bmatrix} \quad (20)$$

The digraph is drawn as shown in Fig. 7

From the digraph the reachability condition for controllability is satisfied if any one or more of the states: 4,5,6, are directly influenced by the control actuators. The term rank of $\bar{A}_B$ has a deficiency of two and thus two actuators are required for controllability. Even if the damping matrix D=0, the same number (2) of actuators is needed for controllability and, thus, it is shown that damping has no effect on the required number of actuators. But, if the damping matrix D=0, then the location of the actuators must be changed such that the states 4,5&6 can be directly influenced by the control actuators. In order to emphasize the point, when D=0 the dotted lines should be removed from the digraph shown in Fig. 7.

VI. Conclusions

The definition of controllability as applied to general linear time invariant dynamics systems and large space systems is reviewed. The special nature of the coupled matrix second order differential equations that are used to describe large space systems is used to arrive at specific controllability conditions. The graph theory approach is employed to define controllability in terms of the term rank and input-state reachability concepts. This approach is used to find the effect of inherent damping present in large space systems on the number of the actuators and their locations. It is observed that the damping does not affect the minimum number of actuators required, but does provide greater flexibility in the possible locations of the actuators. The number of actuators reqired depends on the term rank of the generalized system (stiffness) matrix. The stiffness matrix also influences the location of the actuators.

References

1. Kalman, R.E., "On the General Theory of Control Systems," in Proc. 1st IFAC Congress, vol. 1, London: Butterworth, 1960, pp. 481-491.

2. Paige, C.C., "Properties of Numerical Algorithms Related to Computing Controllability," IEEE Trans. on Automatic Control, vol. AC-26, No. 1, Feb. 1981, pp. 130-138.

3. Klema, V.C., and Laub, A.J., "The Singular Value Decomposition: Its Computation and Some Applications," IEEE Trans on Automatic Control, vol. AC-25, No. 2, April 1980, pp. 164-176.

4. Balas, M.J., "Feedback Control of Flexible Systems," IEEE Trans. on Automatic Control, vol. AC-23, No. 4, Aug. 1978, pp. 673-679.

5. Schizas, C., and Evans, F.J., "Rank Invariant Transformations and Controllability of Large Scale Systems," Electronic Letters, vol. 16, No. 1, 3rd Jan., 1980., pp. 19-20.

6. Kumar, V.K., and Bainum, P.M., "On the Motion of a Flexible Shallow Spherical Shell in Orbit," AIAA 19th Aerospace Sciences Meeting, Jan. 12-15, 1981, St. Louis, Missouri, paper no. AIAA-81-0170; also to appear in AIAA Journal.

7. Bainum, P.M., and Reddy, A.S.S.R., "On the Shape and Orientation Control of an Orbiting Shallow Spherical Shell Structure," to be Presented at the Joint IFAC/E.A Symposium on Automatic Control in Space, Noordwijkerhout, the Netherlands, July 5-9, 1982.

Appendix

A. Term Rank of a Matrix

The term rank of a square matrix of dimension $n \times n$ is less than n if and only if the matrix has a zero submatrix "O" of dimension $r \times r'$ with $r \times r' > n$. The term rank is different from the numerical rank in the following sense. If a square matrix of order n has two columns or rows that are dependent on each other, then its term rank is not reduced while its numerical rank is reduced by one for each pair of columns or rows that are dependent. For large space systems, the determination of the numerical values of the elements for the system matrices are not exact, and thus the probability that two columns or rows would be identically equal, or that one row is a constant times another is very small. If such a dependency exists that must be detected before subjecting it to the term rank tests for establishing the controllability of large space systems.

B. Input-State Reachability Matrix

The augmented adjacency matrix for the system matrix pair [A,B] can be written as

$$
C_B = \begin{array}{c} n \\ - \\ m \end{array}
\left[
\begin{array}{c|c}
A_B & B_B \\
\hline
0_{m \times n} & I_{m \times m}
\end{array}
\right]
$$

where A_B and B_B are the adjacency matrices of A and B, respectively.

The states can be reached from any of the inputs and can not be of length more than n. So C_B can be raised to the power n and thus the augmented system reachability matrix is given by

$$
R = \left[
\begin{array}{c|c}
A_B^n & (A_B^{n-1}+A_B^{n-2}+...+A_B)B_B \\
 & (= R_{IS}) \\
\hline
0 & 0
\end{array}
\right] = C_B^n
$$

where R_{IS} is the input-state reachability matrix For all the states to be reached from at least one input, every row of R_{IS} must have at least one non zero entry.
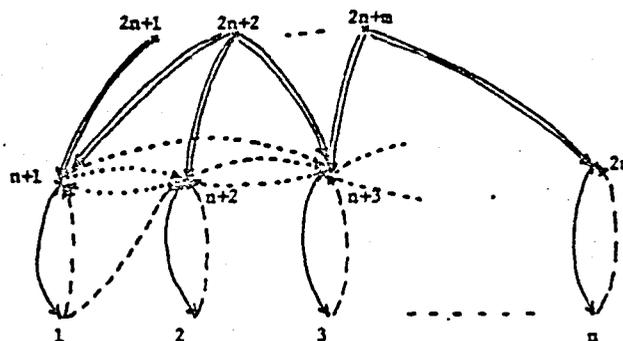

Fig. 1. Digraph of [A,B] matrix pair.
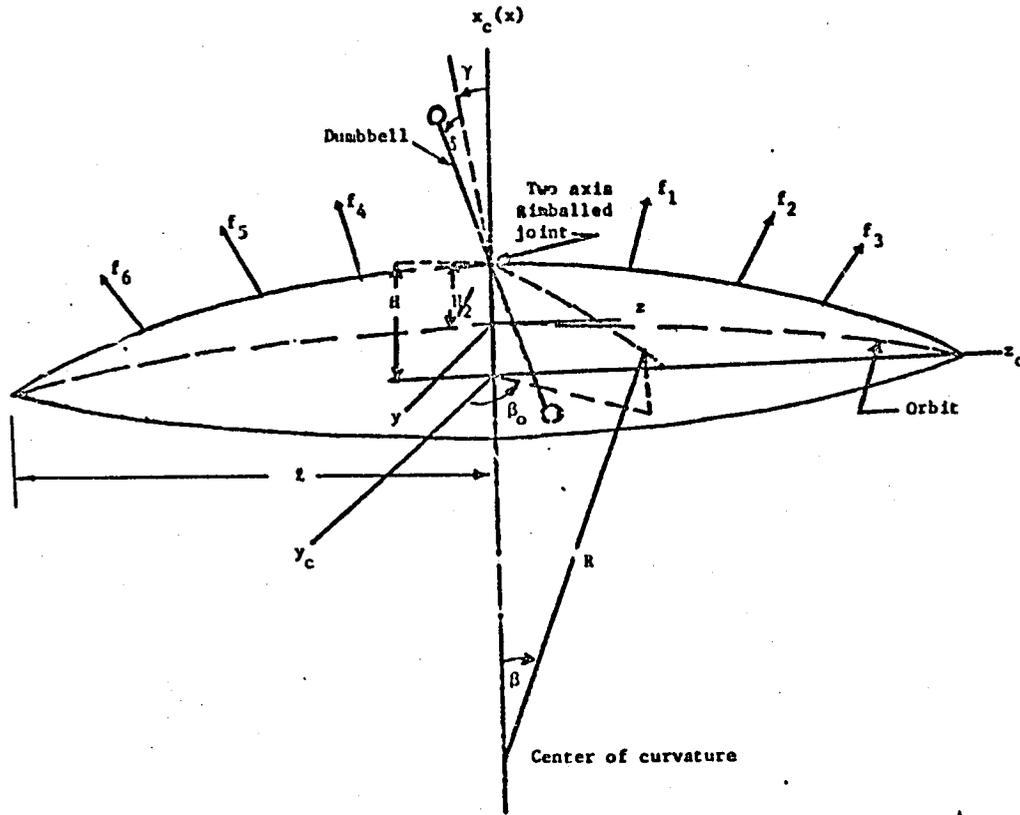
Fig. 2. Shallow spherical shell with dumbbell and actuators.

	1	2	3	4	5	6	7	8	9	10	11	12	13	14	15	16	17	18
1										X								
2											X							
3												X						
4													X					
5														X				
6															X			
7																X		
8																	X	
9																		X
10											X							
11	X									X								
12		X											X	X	X			
13			X										X					
14				X									X					
15						X							X					
16							X											
17								X										
18									X									

Fig 3. Location of non-zero elements in the system matrix of the shallow spherical shell without the dumbbell in orbit

Fig. 4. Digraph of the shallow spherical shell system matrix.

3.7

Fig 5. Location of non-zero elements of the system matrix of the
shell with the dumbbell in orbit.
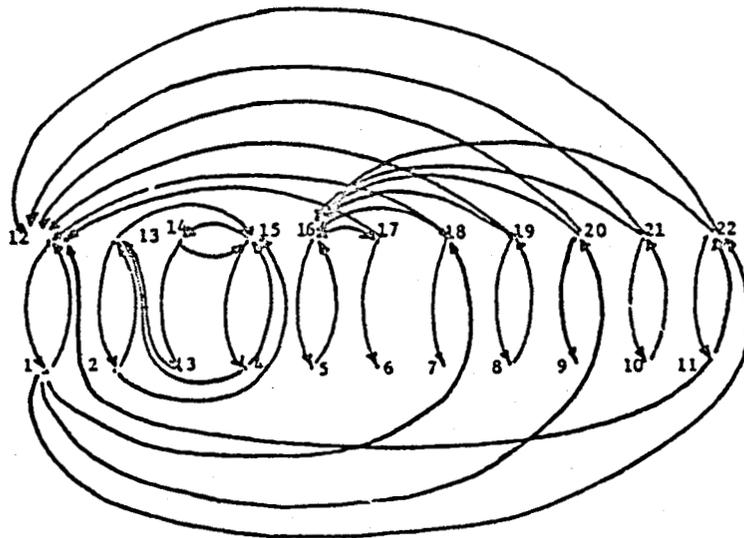
Fig 6. Digraph of the shallow spherical shell system matrix with dumbbell.
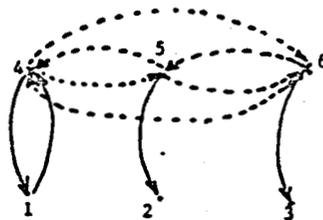

Fig 7. Digraph of system matrix given in equation (20)

3.9

IV. EFFECT OF SOLAR RADIATION DISTURBANCE ON A FLEXIBLE BEAM IN ORBIT

IV.1 INTRODUCTION

Proposed future applications of large space structures require control of the shape and orientation of the structure in orbit. The principal environmental disturbance acting on these structures at the proposed operational altitudes are due to the solar radiation pressure. Therefore, it is necessary to evaluate the solar radiation pressure effects on the large space structures in orbit in order to provide control of their shape and orientation. As a specific example of a basic structure, a long flexible beam constrained to move only in the orbital plane is considered in this study.

The equations of motion for a long flexible beam oriented along the local vertical were obtained previously.[1] Later, the work of Ref. 1 was extended to consider the motion and stability of the beam about a nominal local horizontal orientation. This system includes a rigid dumbbell used for gravitational stabilization that is connected to the center of mass of the beam through a gimballed passive damping device.[2] The control aspects of such a beam using point actuators were also considered in Ref. 3. The effect of solar radiation pressure on the dynamics of these two types of beam structures is studied here, and to the authors' knowledge represents the first time that solar disturbance torques acting on large flexible space systems have been treated.

The force and moment expressions obtained by Karymov[4] are used to develop the solar radiation disturbance model for a beam by considering the individual mode shapes of the free-free beam. The transverse elastic displacements are assumed to be small so that the shadowing of the beam due to any deflected part of the beam can be neglected.

IV. 2 DETERMINATION OF SOLAR RADIATION FORCES AND MOMENTS ACTING ON A FLEXIBLE BEAM

Let the direction of the incident solar radiation, $\bar{\tau}$, in the body coordinate system be denoted as

$$\bar{\tau} = a_o\bar{i} + b_o\bar{j} + c_o\bar{k} \tag{4.1}$$

and, let $\bar{n}$ be the outward unit vector normal to the surface, ds, of a body of arbitrary shape exposed to solar radiation (Fig. 4.1). Then, the solar radiation force acting on a completely absorbing surface, $\bar{F}_a$, and that acting on a completely reflecting surface, $\bar{F}_r$, can be obtained as[4],

$$\bar{F}_a = h_o\bar{\tau} \int_s \bar{\tau} \cdot \bar{n} \, ds \tag{4.2}$$

and

$$\bar{F}_r = -2h_o \int_s \bar{n}(\tau \cdot \bar{n})^2 ds \tag{4.3}$$

where, $h_o = 4.64 \times 10^{-6} N/m^2$ is a constant for earth orbiting spacecraft and the integration over an area, s, is bounded by the condition

$$\bar{\tau} \cdot \bar{n} \geq 0 \tag{4.4}$$

The corresponding moments for a completely absorbing surface, $\bar{N}_a$, and for a completely reflecting surface, $\bar{N}_r$, respectively, can be developed as[4],

$$\bar{N}_a = h_o\bar{\tau} \times \int_s \bar{R}(\bar{\tau} \cdot \bar{n}) ds \tag{4.5}$$

$$\bar{N}_r = 2h_o \int_s \bar{n}x\bar{R}(\bar{\tau} \cdot \bar{n})^2 ds \tag{4.6}$$

where $\bar{R}$ is the position vector of ds with respect to the center of mass. For a a surface with an arbitrary reflection coefficient, ϵ_r, the force and moment expressions become[4]:

$$\bar{F}_{\epsilon r} = \bar{F}_a + \epsilon_r(\bar{F}_r - \bar{F}_a) \tag{4.7}$$

$$\bar{N}_{\epsilon r} = \bar{N}_a + \epsilon_r(\bar{N}_r - \bar{N}_a) \tag{4.8}$$

The forces and moments due to solar radiation pressure acting on a free-free flexible beam can now be obtained by considering the shape function of the beam, ϕ, (Fig. 4.1, only the first anti-symmetric mode is depicted). The beam is assumed to vibrate in the transverse direction only so that the normal at any point is given by

$$\bar{n} = (\phi'\bar{i} - \bar{k}) / \sqrt{1 + \phi'^2} \tag{4.9}$$

where $\phi' = \dfrac{d\phi}{d\xi}$ and ξ is the nondimensionalized longitudinal coordinate of the beam with the elemental length,

$$ds = d\xi\sqrt{1 + \phi'^2} \tag{4.10}$$

If the analysis is restricted to a single plane containing ξ and ζ $\bar{\tau}$ reduces to

$$\bar{\tau} = a_o\bar{i} + c_o\bar{k} \tag{4.11}$$

using Eqs. (4.9), (4.10), and (4.11) in Eq. (4.2), the total force acting per unit width of the beam is expressed as

$$\bar{F}_a = -h_o\bar{\tau} \int_o^1 (a_o\bar{i} + c_o\bar{k}) \cdot (\phi'\bar{i} - \bar{k})d\xi$$

$$= a_o c_o h_o\bar{i} + h_o c_o^2\bar{k} \quad \text{(for symmetric modes)} \tag{4.12}$$

$$= -h_o(2a_o\delta_o - c_o)(a_o\bar{i} + c_o\bar{k}) \quad \text{for asymmetric modes)}$$

where, $\delta_o = \phi_z^n(0) = $ deflection at one end of the beam for the nth mode. The total force per unit width of the beam acting on a completely reflecting surface is obtained after substituting Eqs. (4.9), (4.10) and (4.11) in Eq. (4.3) as

$$F_r = -2h_o \int_o^1 \frac{(a_o\phi' - c_o)^2}{(1 + \phi'^2)} (\phi'\bar{i} - \bar{k})d\xi \tag{4.13}$$

4.3

The expressions for the moments per unit width of the beam are developed

using Eqs. (4.9), (4.10) and (4.11) in Eqs. (4.5) and (4.6) as:

$$\bar{N}_a = h_o \bar{\tau} x [\int_o^1 (a_o\phi'-c_o)\{(\xi-\tfrac{1}{2})\bar{i}+\phi\bar{k}\} \, d\xi$$

$$= -h_o a_o c_o [\delta_o - 2\int_o^1 \phi(\xi)d\xi] \quad \text{(for symmetric modes)} \qquad (4.14)$$

$$= 2h_o a_o c_o \int_o^1 \phi(\xi)d\xi \qquad \text{(for asymmetric modes)}$$

$$\bar{N}_r = 2h_o \int_o^1 \frac{(a_o\phi'-c_o)^2}{(1+\phi'^2)} \quad (\phi'\bar{i}-\bar{k})\times\{(\xi-\tfrac{1}{2})\bar{i}+\phi\bar{k}\} \, d\xi$$

$$= -2h_o \int_o^1 \frac{(a_o\phi'-c_o)^2}{(1+\phi^2)} \{\phi'\phi+(\xi-\tfrac{1}{2})\} \, \bar{j} \, d\xi \qquad (4.15)$$

Eqs. (4.13) and (4.15) involve complicated line integrals. These integrals

can be evaluated using numerical integration methods. For the purpose of

this numerical study a beam of length 100 meters with tip deflections of

(i) 0.01ℓ and (ii) 0.1ℓ were considered. Fig. 4.2 shows the variation of

the resultant horizontal and normal force components of a beam with a

completely absorbing surface as the solar incidence angle, θ_i, is varied

from 0 to 90 degrees. Here, θ_i represents to angle between the normal

to the undeflected beam and $\bar{\tau}$. The horizontal and normal force components

are measured relative to the beam's undeflected axes. As expected, for

small tip deflections of the beam, the resultant horizontal absorbing

force component becomes zero for incidence angles of 0 and 90 degrees,

respectively, while the normal component has a maximum amplitude at zero

incidence angle. In Fig. 4.2 and subsequent figures the individual effect

of each mode, with the assumed beam tip deflection as indicated in the figure,

is illustrated.

4.4

Fig. 4.3 shows the force distribution along the length of the beam deflected in the first mode due to the solar radiation incident at an angle of 45°. The asymmetric nature of the force distribution gives rise to a resultant moment about the center of mass of the beam. The magnitude of the resultant moments as the solar incidence angle is varied is shown in Fig. 4.4 for each symmetric mode and the assumed tip deflection. Large moments can result for larger deflections whereas these moments would be zero for a rigid beam. Because the force distribution for an asymmetric mode is symmetric about an axis passing through the mass center and parallel to the incident solar radiation, the moments for all asymmetric modes are zero (Fig. 4.3). For small pitch angle displacements, the moment due to solar radiation pressure may become greater than the moment due to the gravity-gradient forces as shown in Fig. 4.5. It is seen that at geosynchronous altitudes, the moment due to solar radiation may become predominant even for deflections of the order of 0.01ℓ.

Figs. 4.6,4.7, and 4.8 show the forces and moments for a completely reflecting surface, obtained using numerical integration techniques based on Eqs. (4.3) and (4.6). It is seen that the moment for the completely reflecting case increases with the larger value of the tip deflection. Since the radiation force acts along the normal to the surface for a completely reflecting surface, and the deflections of the beam are assumed small, the normal force components are seen to be much greater than the horizontal force components (Fig. 4.6). Further, the resultant force components also depend on the mode shapes (Fig. 4.7) in contrast to the case of the completely absorbing surace (Fig. 4.2).

4.5

Hence, the moments for the reflecting beam also depend on the specific mode
number of the beam incorporated into the model as shown in Fig. 4.8. Because
of symmetric force distribution about the center of mass the resultant moment
is zero for all asymmetric modes as before. Hence, the moments are zero for
all asymmetric modes regardless of the surface reflectivity. For the higher
symmetric modes of the reflecting beam the resultant moments are seen to
decrease because of the greater scattering associated with sharper changes
in the beam slope.

With the aid of these moment diagrams, it is now possible to model the
disturbance torque due to solar radiation pressure, once the number of modes
and the associated modal deflections are specified. This aspect is considered
in the next section.

IV.3 SOLAR RADIATION DISTURBANCE MODEL

A beam nominally oriented along the local horizontal or local vertical is considered. Such a beam makes one revolution per orbit with respect to the incident solar radiation. For any symmetric mode and for a given coefficient of reflectivity, ϵ_r, the pitch torque can be expressed as a function of the solar incidence angle, θ_i, in the form [from Figs. 4.4 and 4.8],

$$N = N_m \sin\theta_i \cos\theta_i$$

where,
$$N_m = N_{a_m} + \epsilon_r (N_{r_m} - N_{a_m}) \tag{4.16}$$

N_{a_m}, N_{r_m} = maximum moment per unit deflection for a completely absorbing surface (from Fig. 4.2) and for a completely reflecting surface (from Fig. 4.8), respectively.

For small deflections, N is proportional to the deflection at one end of the beam, $\delta(t)$, or the nondimensionalized parameter, $\epsilon_n(t) = \dfrac{A_n(t)}{\ell}$, where $A_n(t)$ = modal amplitude function.

$$N(t) = \epsilon_n(t) N_m \ell \sin\theta_i \cos\theta_i \tag{4.17}$$

and θ_i is given by

$$\theta_i(t) = \omega_c t + \theta(t) + \theta_i(0) \tag{4.18}$$

where, ω_c is the orbital angular velocity, and θ is the pitch angle of the beam.

The effect of the disturbance on the generic mode is obtained by evaluating the integral

$$E_n = \int \overline{\phi}^{(n)}(\xi) \cdot \overline{e} \, ds \tag{4.19}$$

where, $\overline{e}$ is the external force.

Eqs. (4.2) and (4.3) are substituted into Eq. (4.19) to obtain

$$E_{n_a} = \int \overline{k}\phi_z^{(n)} \cdot \{h_o \overline{\tau}(\overline{\tau} \cdot \overline{n})\} \, ds$$

$$= h_o c_o^2 \int_o^1 \phi_z^{(n)} d\xi \tag{4.20}$$

4.7

and
$$E_{n_r} = \int \bar{k}\phi_z^{(n)} \cdot \{-2h_o(\bar{\tau}\cdot\bar{n})^2\} \, ds \qquad (4.21)$$

$$= 2h_o c_o^2 \int_o^1 \phi_z^{(n)} \, d\xi$$

After combination of Eqs. (4.19) and (4.20), the generic force is obtained
as,
$$E_n = E_{n_a} + \epsilon_r(E_{n_r} - E_{n_a})$$

$$= h_o c^2(1+\epsilon) \int_o^1 \phi_z^{(n)} \, d\xi \qquad (4.22)$$

For $\epsilon_r = 0.5$ and a tip deflection of 0.01ℓ, Eq. (4.16) yields

$$N_m = 2.23\text{x}10^{-4} + 0.5(9.4\text{x}10^{-5} - 2.23\text{x}10^{-4})$$

$$= 1.58\text{x}10^{-4} \text{ N-m}$$

This is the maximum torque that is experienced by the beam for a unit de-
flection equal to 1m. in a 100m. length beam at any instant in the orbit.
The corresponding generic forces on each mode with a tip deflection of 0.01ℓ
in the respective modes are obtained (from Eq. (4.22), for the first four
mods, as

$$E_1 = 0.159\text{x}10^{-6} \text{ N}$$
$$E_2 = 0.827\text{x}10^{-9} \text{ N}$$
$$E_3 = 0.102\text{x}10^{-8} \text{ N}$$
$$E_4 = 0.3432\text{x}10^{-8} \text{ N}$$

Thus, the generic forces are seen to be very small and, hence, the modal
excitations due to solar radiation pressure are also small. However, the
magnitude of the solar radiation torques indicate that considerable pitch
rotations can be expected for larger deflections of the beam. The numerical
values for E_n and N_m are used in the two examples in the following sections.
In the first example a beam nominally oriented along the local vertical
(Fig. 4.9) is considered. Next, a beam nominally oriented along the local
horizontal and gravitationally stabilized by a rigid dumbbell (Fig. 4.10)
is considered.

IV.4 EFFECT OF SOLAR RADIATION PRESSURE ON A FLEXIBLE BEAM NOMINALLY ORIENTED ALONG THE LOCAL VERTICAL

The equations of motion for a thin uniform beam in orbit with its axis nominally along the local vertical (Fig. 4.9) is developed in Ref. 2. The beam is assumed to undergo only inplane angular motions and deformations and it is assumed also that the center of mass of the beam follows a circular orbit. The beam's elastic motions are considered to be unconstrained and the longitudinal vibrations of the beam are assumed to be negligible in comparison with the transverse vibrations. For the case of small amplitude pitch oscillations of the beam, the linearized equations of motion are derived as[2]

$$\theta'' + 3\theta = {}^{N}/J\omega_c^2$$

$$\epsilon_n'' + \omega_n^2 \epsilon_n = \frac{E_n}{M_n \ell \omega_c^2} \qquad (4.23)$$

where,
$\quad \theta$ = pitch motion of the beam

$\quad \epsilon_n = \dfrac{A_n}{\ell}$ = non dimensionalized modal amplitude

$\quad n$ = mode number

$\quad J$ = pitch moment of inertia of the beam

$\quad N$ = external torque

$\quad E_n$ = nth modal force

$\quad M_n$ = nth modal mass

$\quad \omega_c$ = orbit angular velocity

$\quad \omega_n = \dfrac{\Omega_n}{\omega_c}$, Ω_n = nth modal frequency

$\quad (\ )' = \dfrac{d}{d\tau}$

$\quad \tau = \omega_c t$, nondimensionalized time parameter

$\quad t$ = time

4.9

Only the first two flexural modes of the beam will be included in the analysis. Using Eqs. (4.17) and (4.22) and the numerical values for N_m, E_1 and E_2, the following three equations of second order result.

$$\theta'' + 3\theta = 3.6\, \varepsilon_1\, \sin\theta_1\, \cos\theta_1$$

$$\varepsilon_1'' + \omega_1^2 \varepsilon_1 = 3.001 \times 10^{-2}\, \varepsilon_1\, \cos^2\theta_1$$

$$\varepsilon_2'' + \omega_2^2 \varepsilon_2 = 1.563 \times 10^{-4}\, \varepsilon_2\, \cos^2\theta_1 \qquad (4.24)$$

The second modal oscillation is seen to be decoupled from the first mode and pitch motions. Further, the forcing terms in the first and second modes are very small and can be neglected to first order. Therefore, ε_1 and ε_2 have solutions of the form

$$\varepsilon_1 \cong c_1 \sin\omega_1 \tau + c_2 \cos\omega_1 \tau$$

$$\varepsilon_2 \cong c_3 \sin\omega_2 \tau + c_4 \cos\omega_2 \tau \qquad (4.25)$$

where c_1, c_2, c_3 and c_4 are constants to be determined from the initial conditions. The pitch equation now becomes

$$\theta'' + 3\theta = 1.8\, (c_1 \sin\omega_1 \tau + c_2 \cos\omega_1 \tau)\, \sin2\theta_1$$

Assuming $\qquad \theta_1(0) = 0$ and $\theta(t)$ very small

$$\theta_1(t) = \omega_c t = \tau \text{ from Eq. (4.18)}$$

With $\varepsilon_1(0) = \varepsilon_0$ and $\varepsilon_1' = 0$, $c_1 = 0$ and $c_2 = \varepsilon_0$, and the pitch equation becomes

$$\theta'' + 3\theta = 1.8\varepsilon_0 \cos\omega_1 \tau\, \sin2\tau$$

$$= 0.9\varepsilon_0 \{\sin(2+\omega_1)\tau + \sin(2-\omega_1)\tau\} \qquad (4.26)$$

The solution of this equation can be obtained in the form

$$\theta(\tau) = c_5 \sin\sqrt{3}\tau + c_6 \cos\sqrt{3}\tau + \frac{0.9\varepsilon_0}{3-p^2}\, \sin p\tau - \frac{0.9\varepsilon_0}{3-q^2}\, \sin q\tau$$

where, $\qquad p = 2+\omega_1$ and $q = 2-\omega_1$

With $\theta(0) = 0$ and $\varepsilon_1(0) = 0.1$ and $\omega_1 = 10$, the pitch response is given by

$$\theta(\tau) = 0.002392\sin\sqrt{3}\tau + 0.000638\sin12\tau - 0.001475\sin8\tau \qquad (4.27)$$

The response of the beam to the solar radiation disturbance obtained using numerical integration of Eq. (4.24) is shown in Fig. 4.11. The pitch motion shown in Fig. 4.11 is identical with the response obtained using Eq. (4.27) and shows a maximum pitch amplitude of 0.23°. The effect of the disturbance on the first modal oscillations is seen to be negligible.

IV.5 EFFECT OF SOLAR RADIATION PRESSURE ON A DUMBBELL STABILIZED FLEXIBLE BEAM NOMINALLY ORIENTED ALONG THE LOCAL HORIZONTAL

The uncontrolled local horizontal orientation of a beam represents an unstable motion. This unstable configuration of the beam can be stabilized by using a rigid dumbbell such that the resulting gravity-gradient torques provide stabilization. In Ref. 2, the equations of motion for a beam with a dumbbell assumed to be attached at the center of mass of the beam (Fig. 4.10) through a spring loaded hinge and having viscous rotational damping have been developed. In addition to the assumptions made in developing Eqs. (4.23), it is further assumed that the dumbbell mass is concentrated at the tips and that the viscous force at the hinge is linear. With the usual assumptions of small pitch amplitude and dumbbell oscillations and flexural deformations, the linearized equations of motion in the absence of active control and external forces are obtained as[2],

$$\theta'' + \bar{c}\theta' + (\bar{k}-3)\theta - \bar{c}\alpha' - \bar{k}\alpha + \sum_n (\bar{c}\epsilon_n' + \bar{k}\epsilon_n) c_z^{(n)} = \frac{N}{J\omega_c^2} \tag{4.28}$$

$$\alpha'' + c_1\bar{c}\alpha' + (c_1\bar{k}+3)\alpha - c_1\bar{c}\theta' - c_1\bar{k}\theta - \sum_n (\bar{c}\epsilon_n' + \bar{k}\epsilon_n) c_1 c_z^{(n)} = 0 \tag{4.29}$$

$$\epsilon_n'' + (\omega_n^2 - 3)\epsilon_n - \{\bar{k}(\alpha-\theta) + \bar{c}(\alpha'-\theta')\} c_z^{(n)} (J_y/M_n \ell^2) + \sum_m (\bar{c}\epsilon_m' + \bar{k}\epsilon_m) c_z^{(mn)}$$

$$= E_n/M_n \omega_c^2 \ell \tag{4.30}$$

where $c_z^{(mn)} = J_y c_z^{(m)} c_z^{(n)}/M_n \ell^2$; $(m,n = 1,2,\dots)$ and $M_n =$ mass of the beam for all n.

$\bar{k} = k/J_y\omega_c^2$; $\bar{c} = c/J_y\omega_c$

k = torsional restoring spring constant at the hinge

c = viscous damping coefficient

α = angle between the dumbbell axis and the local vertical

$$c_z^{(n)} = \frac{\partial \phi_z^{(n)}}{\partial x} \bigg|_{x=0}$$

$\phi_z^{(n)}$ = beam shape function of the nth transverse mode

c_1 = J_y/I_d I_d = pitch moment of inertia of the dumbbell

As before, only the first two modes will be considered. The forcing terms are the same as for the case of the beam along the local vertical, Eq. (4.24). Since the dumbbell is assumed to be rigid, there is no net moment acting on the dumbbell due too solar radiation pressure. The first mode influences the pitch motion through the forcing function and the second mode affects the dumbbell motion through coupling. Thus, pitch, dumbbell, and the two modes of the beam are all coupled to each other and the resulting system of equations are too complicated to yield analytical solutions. These equations were numerically integrated with initial tip deflections of 0.01ℓ in the first mode and zero initial displacements in θ, α and ϵ_2, respectively (Fig. 4.12). The steady state response shows pitch amplitudes as high as 2°. The first modal oscillations are not greatly affected due to the solar radiation pressure. The second mode is excited because of the dumbbell motion, but the amplitude remains small (maximum $|\epsilon_2|$ = 0.002). The high frequency oscillation in ϵ_2 and in the pitch acceleration, $N/_{J\omega_c^2}$, are suppressed in Fig. 4.12 for the sake of simplicity.

Fig. 4.13 shows the system response for a stiffer beam with ω_1 = 20.0 and the same initial conditions and beam parameters as for the case with ω_1 = 10.0. The maximum pitch amplitude is seen to be about 0.23^o, one order of magnitude less than that for the beam with ω_1 = 10.0.

In this case the higher frequencies in the second mode damp the pitch oscillation, through the dumbbell motion, more rapidly so that the pitch amplitudes do not build up. Once again, ϵ_1 and ϵ_2 motions are not affected to first order because of the solar radiation pressure. Thus, the effect of solar radiation pressure is seen to affect mainly the pitch motion.

Since, the solar radiation incidence angle can change considerably for synchronous orbits, a long time simulation (for about 30 orbits) was carried out accounting for the change in the incident angle due to the Earth's motion around the sun ($\approx 1^o$/day) as shown in Fig. 4.14. It can be seen that errors in both phase and amplitude can result by not including the annual variation in the solar incidence within simulations over long time intervals.

The effect of solar radiation pressure on the pitch response for a different set of inital conditions ($\theta(0) = \alpha(0) = 0$, $\epsilon_1(0) = \epsilon_2(0) = 0.005$) was also obtained (Fig. 4.15). The solid line shows the pitch response without the solar radiation disturbance. The pitch response in this case is due to the coupled motion in ϵ_2, α and θ. Since large amplitude (12°) in pitch motion results, the original non-linear equations of motion were used for this study.[2] The pitch response in the presence of solar radiation pressure (dashed lines in Fig. 4.15) shows a maximum pitch amplitude of about 9°. Thus, as much as 3° difference can result by not including the solar radiation disturbance effect for the assumed parameters of the beam in this study.

Fig. 4.16 shows the effect of solar radiation pressure on a beam which is at a low altitude earth orbit (250 n. miles). The pitch excitation is seen to be very small (0.005^o), as expected, because at the low alitudes the gravity-gradient torques are predominant (Fig. 4.5).

4.14

REFERENCES - CHAPTER IV

1. V.K. Kumar and P.M. Bainum, "Dynamics of a Flexible Body in Orbit,"
    Paper No. 78-1418, AIAA/AAS Astrodynamics Conf., Palo Alto, Calif.,
    August 7-9, 1978; Also in J. of Guidance and Control, Jan.-Feb. 1980,
    Vol. 3, No. 1, pp. 90-92.

2. P.M. Bainum, and V.K. Kumar, "On the Dynamics of Large Orbiting Flexi-
    ble Beams and Platforms Oriented Along the Local Horizontal," XXXI
    International Astronautical Congress, Tokyo, Japan, Sept. 21-28, 1980
    paper No. 80E-230; to appear, Acta Astronautica.

3. P.M. Bainum, R. Krishna and V.K. Kumar, "The Dynamics of Large Flexible
    Earth Pointing Structures with a Hybrid Control System," AAS/AIAA
    Astrodynamics Specialist Conference, Lake Tahoe, Aug. 3-5, 1981, Paper
    No. 81-122; Also to appear in The Journal of the Astronautical Sciences

4. A.A. Karymov, "Determination of Forces and Moments Due to Light Pressure
    Acting on a Body in Motion in Cosmic Space," P.M.M., No. 5, Vol. 26,
   1962, pp. 867-876.
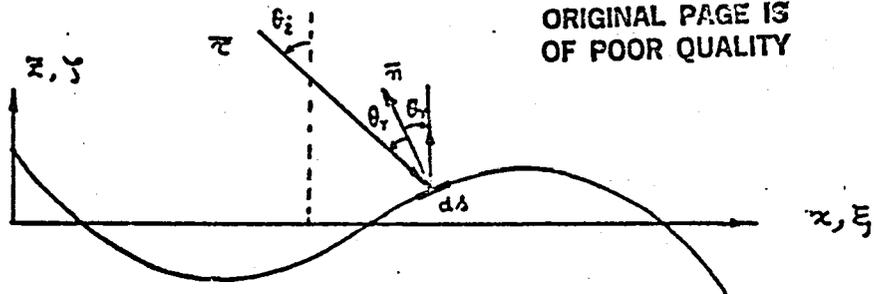
**Fig. 4.1 Geometry of Reflection of a Flexible Beam Exposed to Solar Radiation.**

Rigid Beam and
Symmetric Modes

(a)

(b)

Antisymmetric Modes

Tip Deflection (a) 0.01ℓ
(b) 0.1ℓ

(i) Horizontal Component

Rigid Beam and Symmetric
Modes

(a)
(b)

Antisymmetric Modes

Tip Deflection (a) 0.01ℓ
(b) 0.1ℓ

(ii) Normal Component
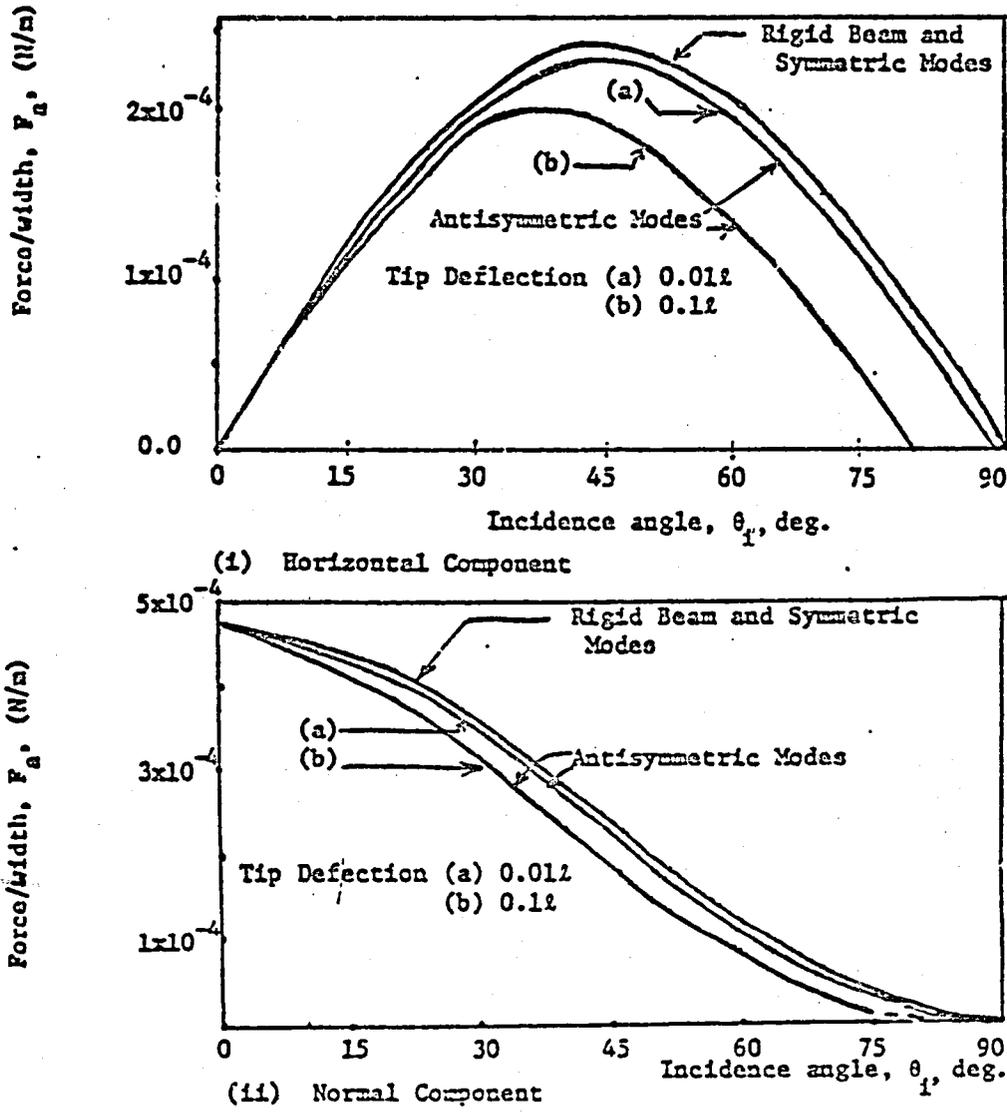
**Fig. 4.2 Variation of Solar Force Components with Incidence Angle
Totally Absorbing Surface - Free-Free Beam (Length, ℓ=100m)**

4.16
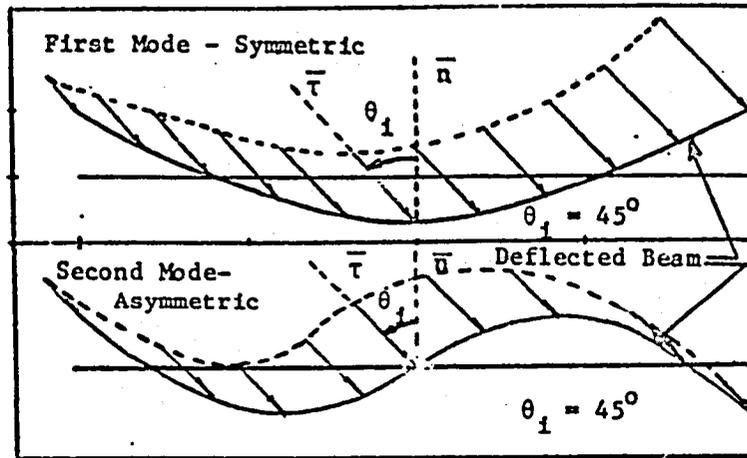
Fig. 4.3   Solar Radiation Force Distribution on the First Two Modes –
Free-Free Beam-Completely Absorbing Surface.
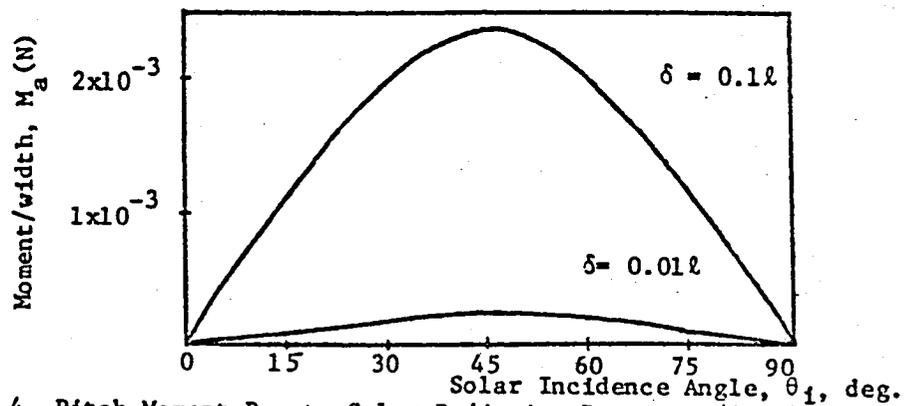
Fig. 4.4   Pitch Moment Due to Solar Radiation Pressure (Completely
Absorbing Surface)-Effect of Each Mode in the System.
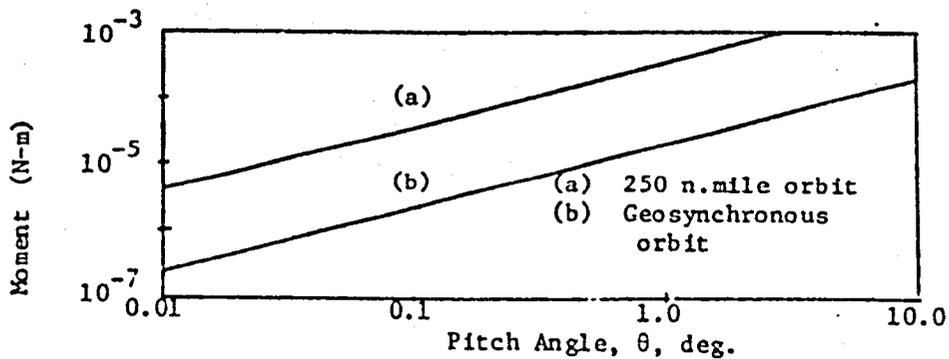
Fig. 4.5   Moment Due to Gravity-Gradient Force as a Function of
Pitch Angle (100m Rigid Beam)

4.17
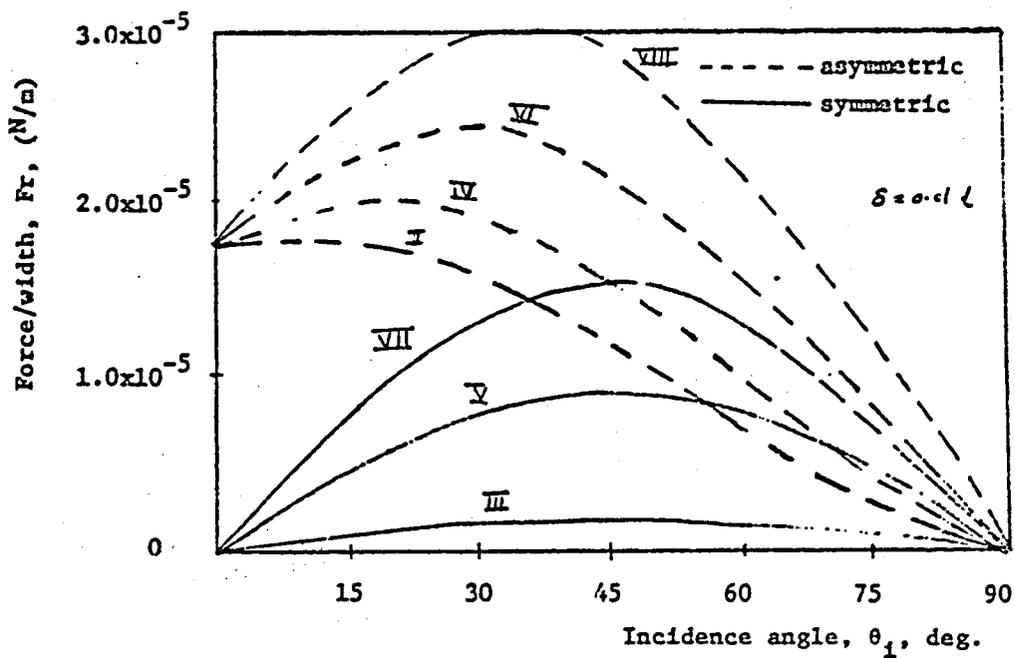
(i) Horizontal Component
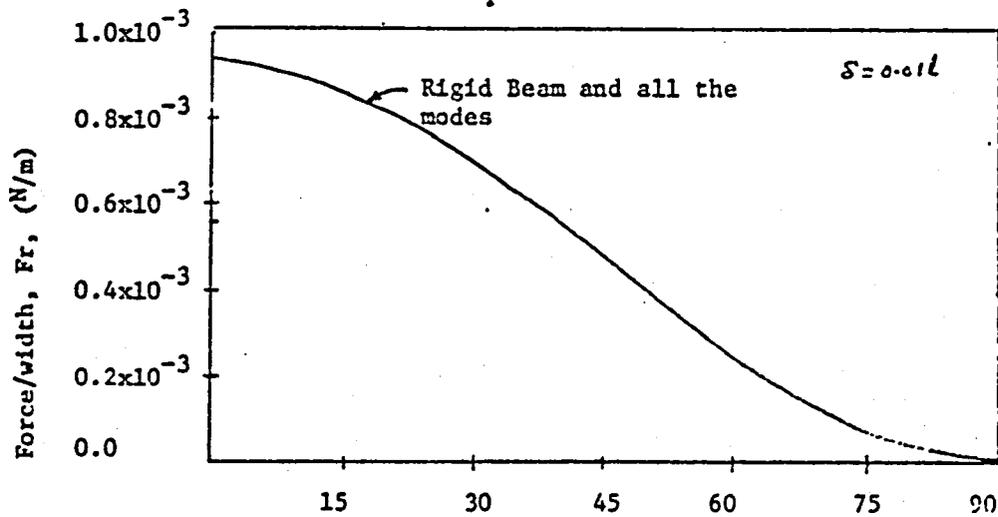
(ii) Normal Component

Fig. 4.6   Variation of Solar Force Components with Incidence
Angle - Totally Reflecting Surface.

(i) Horizontal Component

(ii) Normal Component
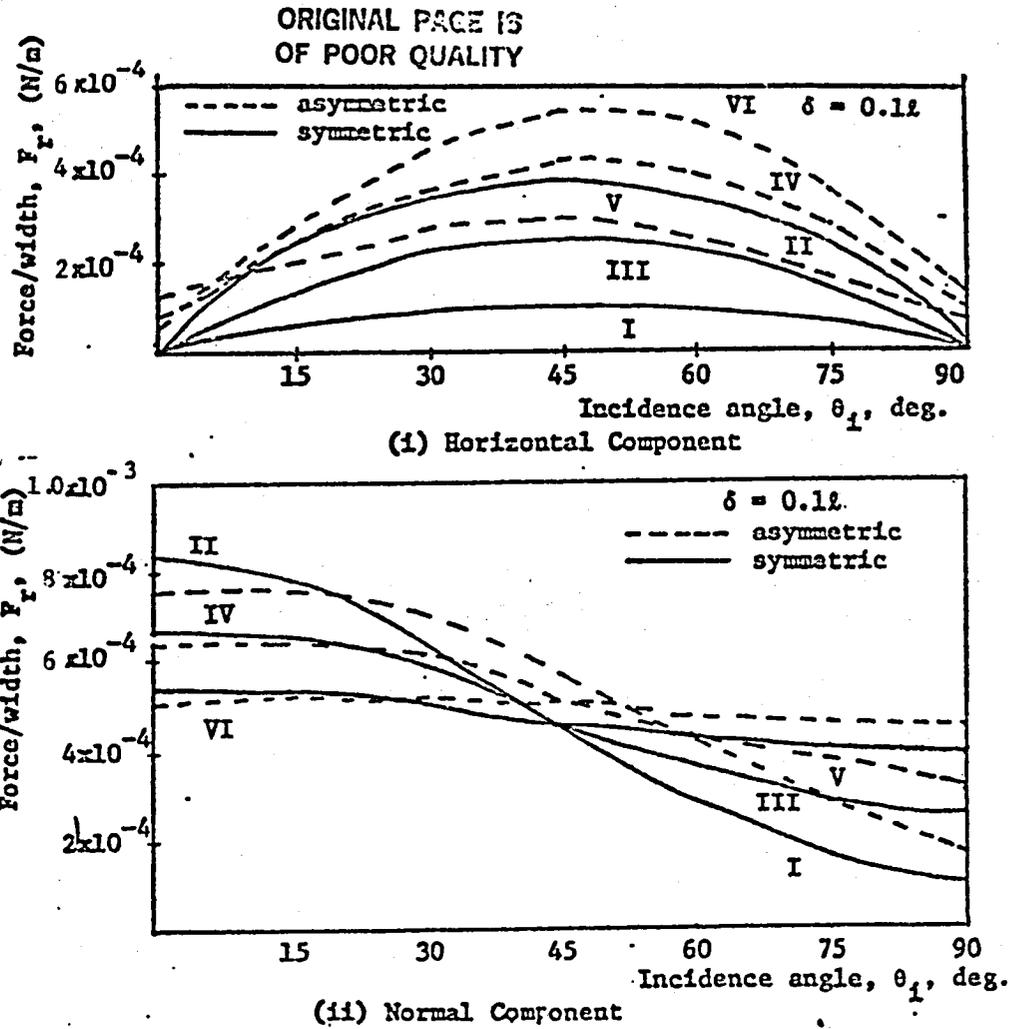
Fig. 4.7. Variation of Solar Force Components with Incidence
Angle-Totally Reflecting Surface
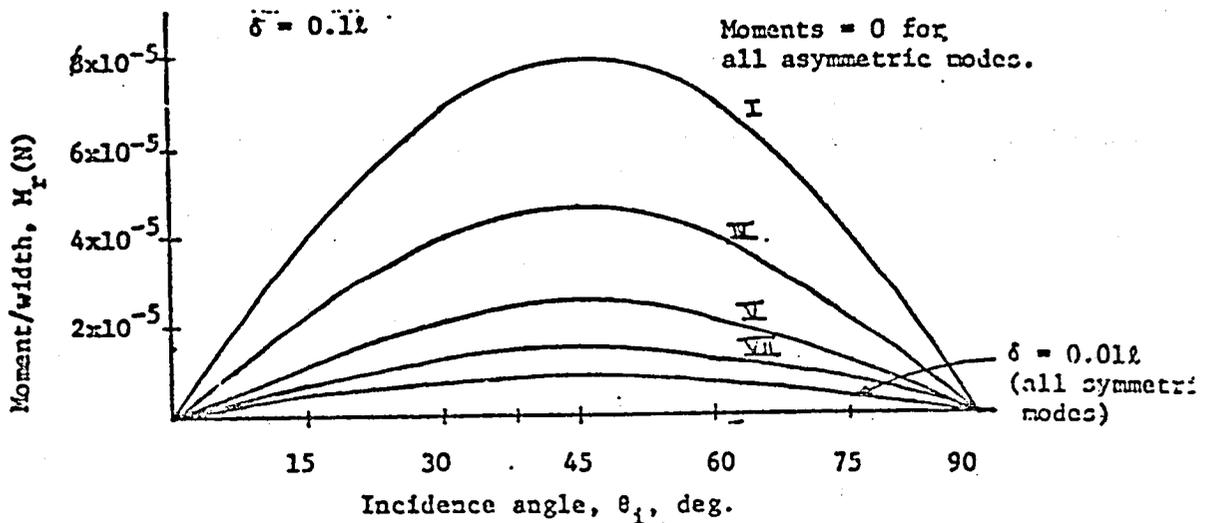
Fig. 4.8 Pitch Moment Due to Solar Radiation Pressure
(Completely Reflecting Surface)
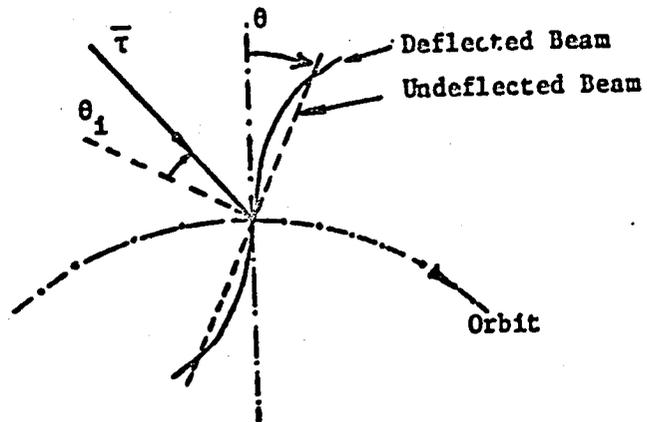
Fig. 4.9.   A Flexible Beam Nominally Oriented Along the Local Vertical
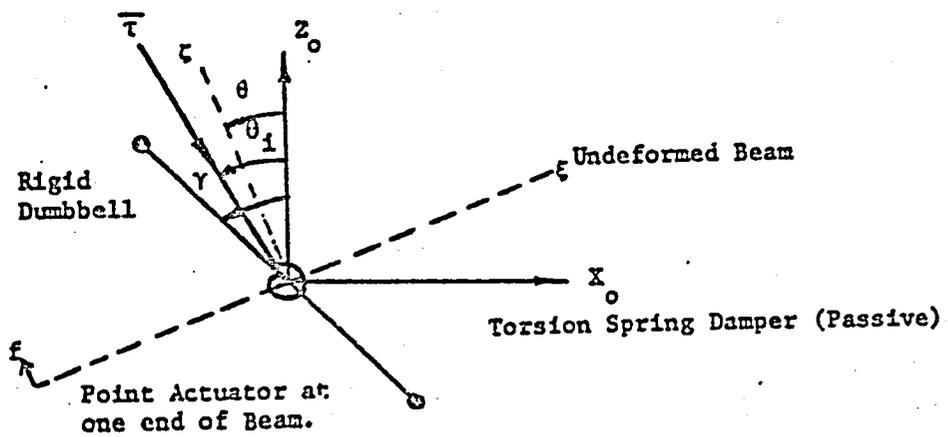
Fig. 4.10 Dumbbell Stabilized Flexible Beam Nominally Oriented Along
the Local Horizontal with Passive and Active Controllers.

Synchronous Altitude

$\omega_1 = 10$ I.C.'s $\theta(0) = \epsilon_2(0) = 0$ $\epsilon_1(0) = 0.01$
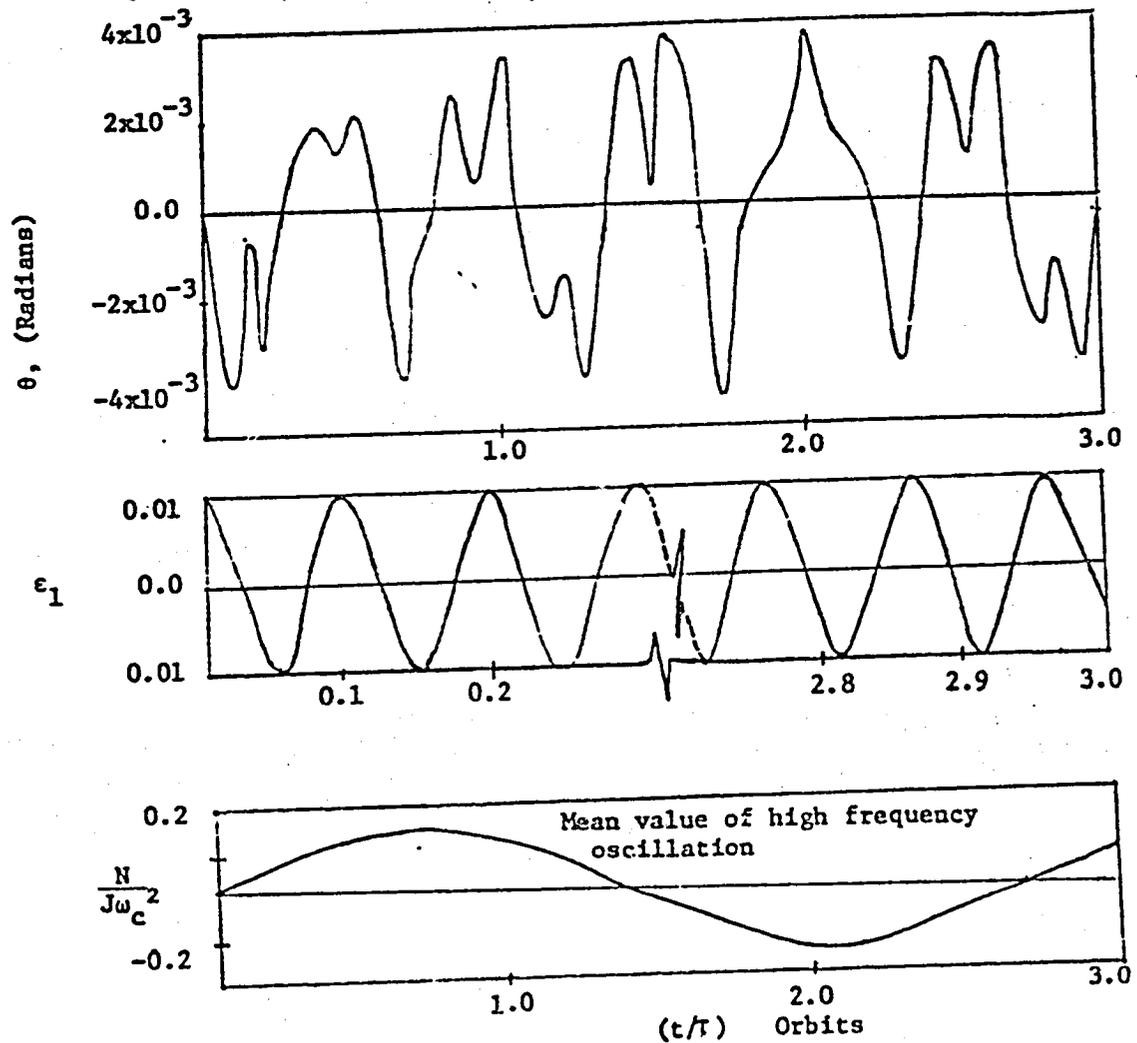
Fig. 4.11 Time Response of the Beam Nominally Along the Local Vertical and in the Presence of Solar Radiation Pressure.

4.21

Synchronous altitude

I.C.'s: $\theta(0) = 0$

$\alpha(0) = 0$

$\epsilon_1(0) = 0.1$

$\epsilon_2(0) = 0$

Mean value of high frequency oscillation

(t/τ) Orbits $\rightarrow$
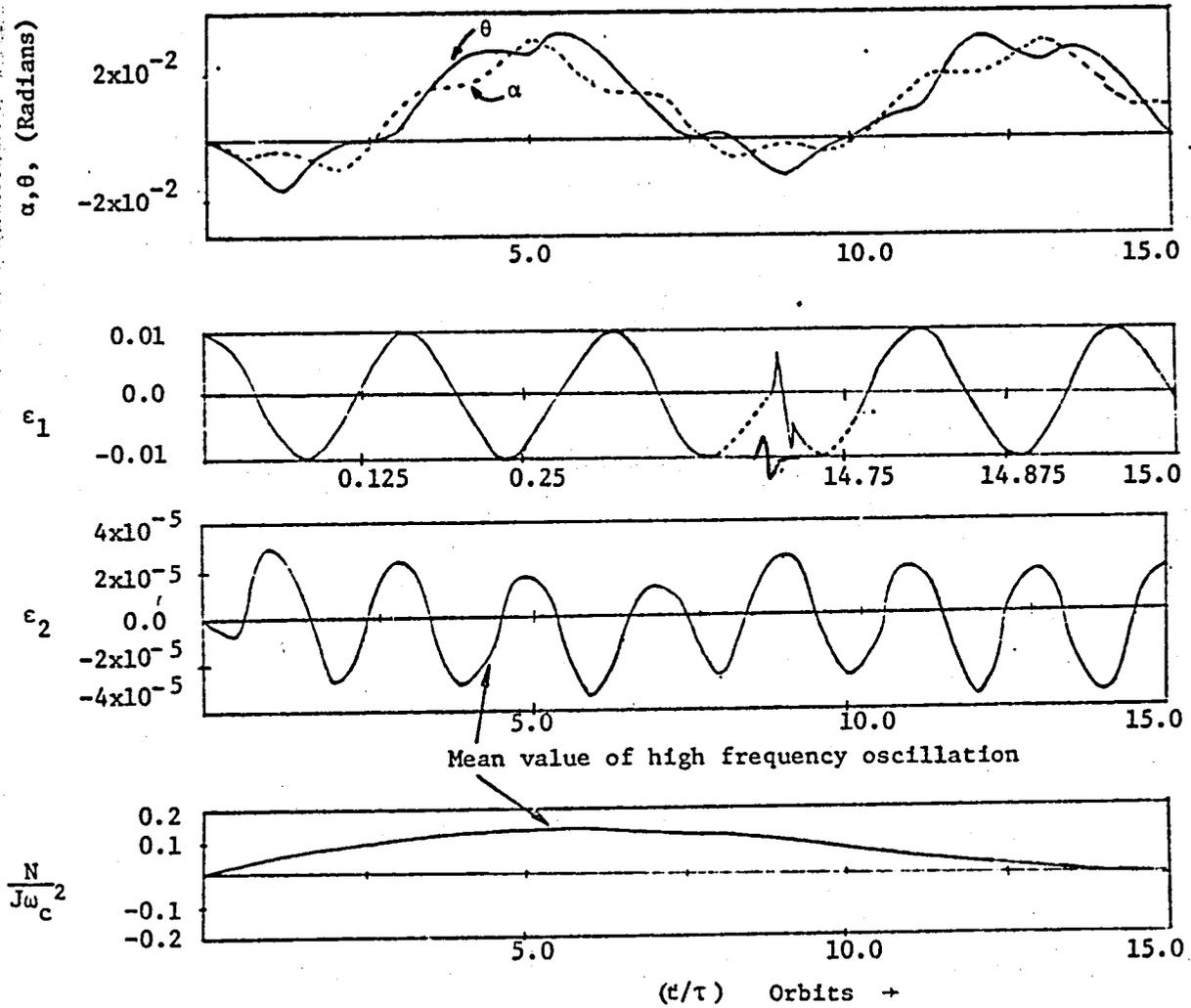
Fig. 4.12.   Time Response of Dumbbell Stabilized Flexible Beam in the
Presence of Solar Radiation Pressure. ($\omega_1 = 10.0$).

4.22

Synchronous altitude

I.C.'s $\theta(0) = 0$
$\alpha(0) = 0$
$\varepsilon_1(0) = 0.1$
$\varepsilon_2(0) = 0$
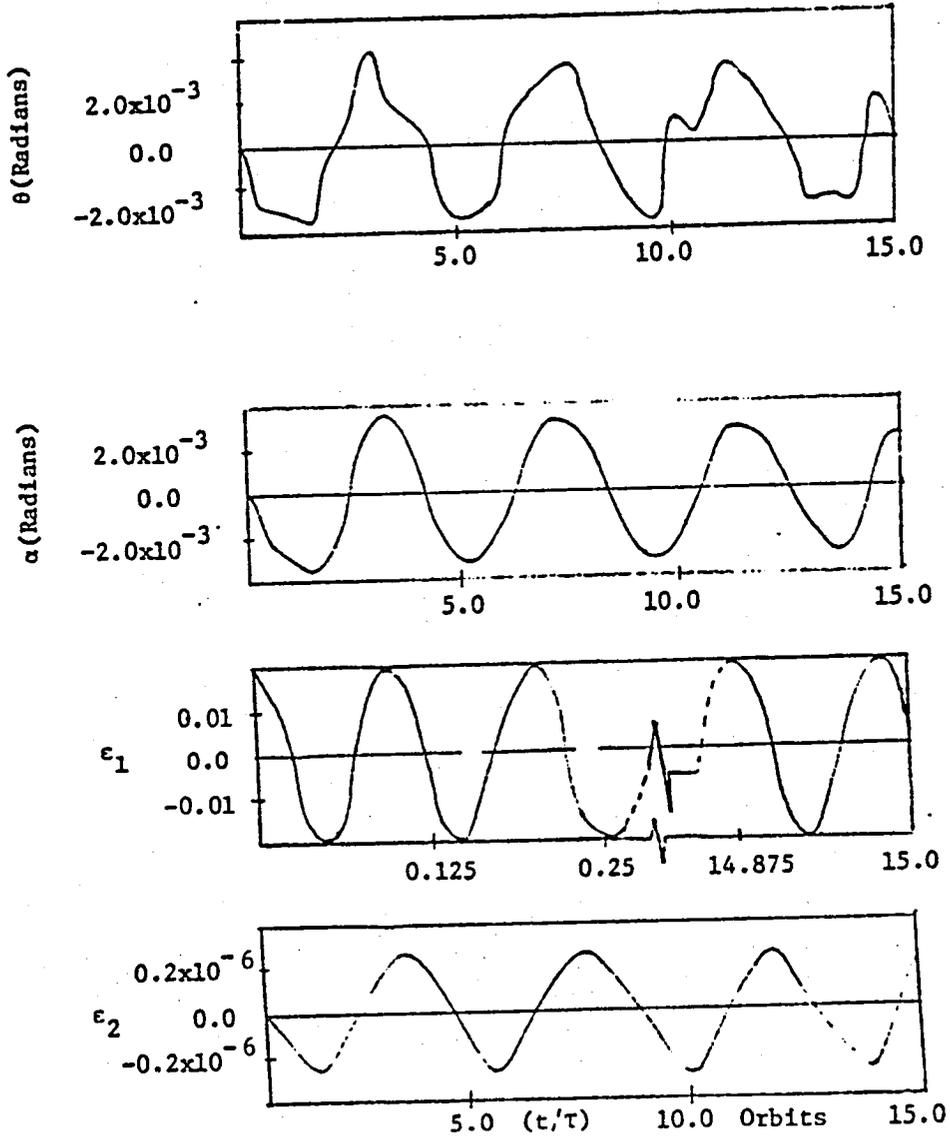
Fig. 4.13. Time Response of Dumbbell Stabilized Flexible Beam in Presence of Solar Radiation Pressure ($\omega_1 = 20.0$).

4.23
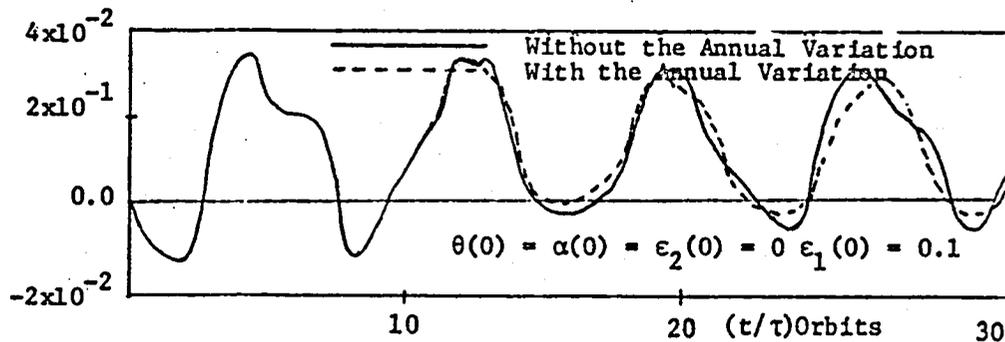
Fig. 4.14   Effect of the Annual Variations in Solar Incidence
Angle- Pitch Response.
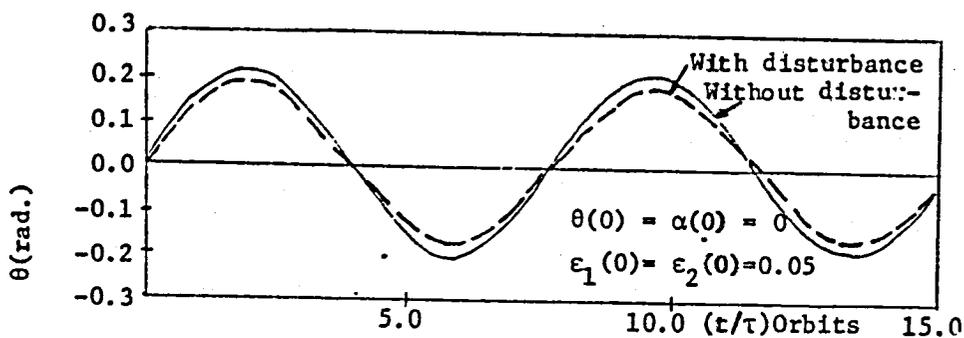
Fig. 4.15   Effect of Solar Radiation Pressure on the Pitch
Response - Initial Condition in the Second Mode Included.
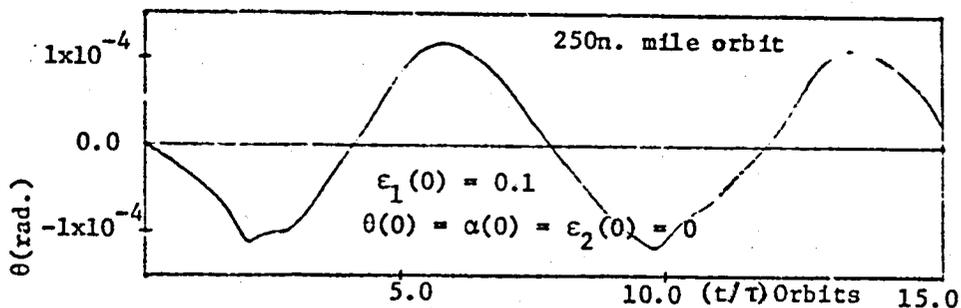
Fig. 4.16   Pitch Response of Dumbbell Stabilized Flexible
Beam in the Presence of Solar Radiation Pressure
at a Low Altitude Orbit.

V. HOOP/COLUMN CONTROLS ANALYSES

V.1 DYNAMIC MODEL OF THE HOOP/COLUMN STRUCTURE

The structural model of the Hoop/Column system shown in Fig. 5.1 is considered for the control analysis. The hoop is assumed to be constructed of five rings with each ring having 24 nodes spaced at 15°. The rings are represented by node numbers 1101-1124, 1201-1224, 1301-1324, 1401-1424 and 1501-1524, respectively. Fig. 5.2 shows a detailed nodal representation of the structure including the mast, (nodes 102-127), feeds, (128-136), and the solar panels, (99-101). The finite element data of the structure provided by the Harris Corporation is used for the controls analysis.

The dynamic model of the structure can be represented as:

$$M\ddot{X} + KX = B_c U \tag{5.1}$$

where X is the state vector containing the generalized coordinates of each node and will be of order (nx6) for n number of nodes and all 6 degrees of freedom. M is the modal mass matrix of order (6nx6n) and K is the stiffness matrix of order (6nx6n). The control matrix, B_c, is of the order of (6nxP) for P number of actuators to be arranged on the structure. The data supplied by Harris Corporation has eigenvectors for 112 nodes and, therefore, n=112 for the present model. To decrease the dimensionality of the problem a modal transformation is carried out, by defining

$$X = \varphi q \tag{5.2}$$

where, ϕ is the matrix containing the eigenvectors of Eq. (5.1) and is of the order (6nxm) for m number of modes and q is a vector of order (mx1).

Through diagonalization of Eq. (5.1) the following matrix equation is obtained.

$$[\phi^T M \phi] \; \ddot{q} + [\phi^T K \phi] \; q = \phi^T B_c U$$

or

$$[\,^{\backprime}m_i\,] \; \ddot{q} + [\,^{\backprime}K_i\,] \; q = \phi^T B_c U \qquad (5.3)$$

where

$$[m_i] = \begin{bmatrix} m_1 & & \\ & m_2 & \\ & & \ddots \\ & & & m_m \end{bmatrix}$$

and

$$[K_i] = \begin{bmatrix} K_1 & & \\ & K_2 & \\ & & \ddots \\ & & & K_m \end{bmatrix}$$

Equation 5.3) is rewritten in the state vector form as

$$\begin{bmatrix} \dot{q} \\ \\ \ddot{q} \end{bmatrix} = \begin{bmatrix} 0 & I \\ \dfrac{-K_i}{m_i} & 0 \end{bmatrix} \begin{bmatrix} q \\ \\ \dot{q} \end{bmatrix} + \begin{bmatrix} 0 \\ \\ [m_i]^{-1} \phi^T B_c \end{bmatrix} \begin{bmatrix} 0 \\ \\ U \end{bmatrix}$$

The values of K_i, m_i and ϕ are available with the finite element model. The evaluation of the control matrix, B_c, for selected actuator locations is discussed in the next section.

V.2   ARRANGEMENT OF ACTUATORS FOR THE HOOP/COLUMN SYSTEM

The controls analysis of the Hoop/Column antenna system requires specification of the type of actuators and their locations and orientations in the structure. For this study point thrusters and/or torquers are assumed to generate the control forces and torques. The location and orientation of these thrusters depend on the mode shapes of the structure. The first thirteen modes corresponding to data provided by the Harris Corp. will be included in the controls analysis and, hence, it is convenient to choose thirteen actuators in the preliminary analysis. Each actuator is selected to affect a particular mode, but the same actuator may help to control a different mode as well. The first six modes are combinations of rigid body rotations and translations. Actuators number 5 and 6 are assumed to be arranged as shown in Fig. 5.3 to provide control over translation along the x and y directions, respectively, and, in addition, also to control the first bending modes (modes 8 and 9). Actuator 11 controls translation along the z direction, whereas actuators 8, 12, and 13 control yaw, pitch and roll motions, respectively. Actuators 1, 2, 3, and 4 are selected so that each actuator could provide independent control of the feed mast torsion (mode 12). Actuators 9 and 10 are selected to control the second mast bending (modes 11 and 13). Actuator 7 controls surface torsion (mode 10) and is the only actuator assumed to be mounted on the hoop. The arrangement of these actuators may need reconsideration for more efficient control performance.

With the selection of m modes in the model, the dimensions of the state matrix, A, becomes $2m \times 2m$ and the corresponding control matrix, B, will be $2m \times p$ for p number of actuators. In the present model, matrix $B = [0 \mid [m_i]^{-1} \phi^T B_c]^T$, where $\phi^T(n,d,m)$ respresents the set of m eigenvectors of the model and,

$$n = \text{number of nodes}$$
$$d = \text{degrees of freedom}$$
$$m = \text{number of modes}$$

ϕ has a dimension of (112, 6, 13) for the present model and for 13 modes. Therefore, the control influence matrix, B_c, will have a dimension of (112, 6, 13) for a total of 13 actuators. The matrix, B_c, results from a finite element formulation of the load (force and moment) matrix and is developed as follows. A column of the matrix, B_c, represents the effect of an actuator on the node at which the actuator is located. For example, actuator 1 located at node 128 (Fig. 5.3) is assumed to provide a force in the y direction only. Hence, the element $B_c(128, 2, 1)$ is set equal to one and the rest of the elements in the coulumn $B_c(n_i, d_j, 1)$ are set equal to zero for each n_i and d_j. The torquer number 8 at node, 98, provides only a yaw moment at node, 98, and so the coulumn $B_c(n_i, d_j, 8)$ contains all zero elements, except at $B_c(98, 6, 8)$ which is set equal to 1. Similarly, the other 11 columns of the influence matrix, B_c, are obtained as shown in Fig. 5.4 in which the matrix, B_c, is arranged as a two-dimensional matrix of order (672, 13). Since there are 13 actuators in this model, only 13 of the (112x6x13) elements of matrix B_c are seen to be non zero.

For 13 actuators located as shown in Fig. 5.3 and Table 5.1, the matrix $[\phi^T B_c]$ is given in Table 5.2. The calculation of the $\phi^T B_c$ was facilitated by the use of a tape containing the ϕ^T elements provided by NASA-LRC.

5.4

V.3 CONTROLLABILITY

To control the finite-element hoop-column model with 13 modes in the model, the minimum required number of actuators is found using graph theory.

Equation (5.3) can be cast into standard state form as:

$$\begin{bmatrix} \dot{q} \\ \ddot{q} \end{bmatrix} = \underbrace{\begin{bmatrix} 0 & I \\ -\dfrac{K_1}{m_1} & 0 \end{bmatrix}}_{A} \begin{bmatrix} q \\ \dot{q} \end{bmatrix} + \underbrace{\begin{bmatrix} 0 \\ [\phi^T B_c] \end{bmatrix}}_{B} \begin{bmatrix} 0 \\ U \end{bmatrix} \qquad 5.4$$

The pair [A,B] in equation (5.4) is controllable if and only if the pair $[[-\dfrac{K_1}{m_1}], [\phi^T B_c]]$ is controllable.[1] From the reachability condition and the digraph shown in Fig. 5.5 for controllability, all the states must be influenced by the inputs directly.

The matrix $[-K_1/m_1]$ has a defficency of 6 in its term rank, as it has a term rank of 7. To augment the term rank, $[\phi^T B_c]$ must have at least six linearly independent non-zero columns, indicating a minimum of six properly placed actuators are needed. A possible set of actuators are (1,2,3,4,5,12) selected from Table 5.1 or Fig. 5.3. On the contrary, the six actuators (1,2,3,4,6,7) from Table 5.1 are not enough to control the thirteen modes in the system as states 14,15 and 26 in the digraph of Fig. 5.5 can not be reached from any of the above six inputs (under the assumption that any element in the $\phi^T B_c$ matrix which is less than 10^{-5} is treated numerically equal to zero).

References Chapter 5

1. Balas, M.J., "Feedback Control of Flexible Systems." IEEE
    Transactions on Automatic Control, Vol. AC-23, No. 4, Aug. 1978,
    pp. 673-679.

2. Schizas, C., and Evans, F.J., "Rank-Invariant Transformations and
    Controllability of Large Scale Systems," Electronic Letters, Vol.
    16, No. 1, 3rd., Jan. 1980, pp. 19-20.

Fig. 5.1 Finite Element Representation of 122m. Hoop/Column System
(One for Two Single Layer Surface Model).
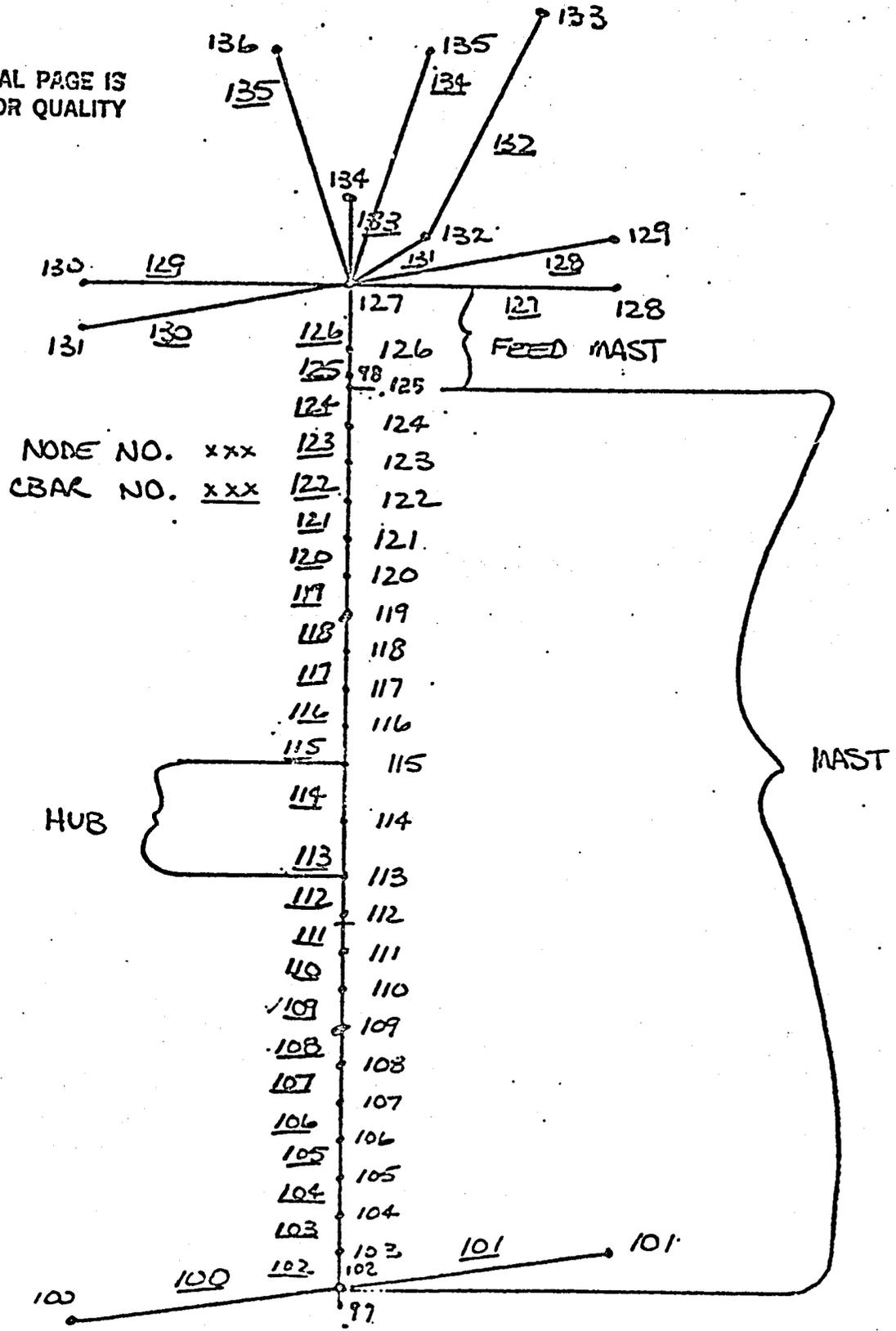
Fig. 5.2 Finite Element Representation of the Mast, Feed, and
Solar Panels - 122m. Hoop/Column System.

5.8
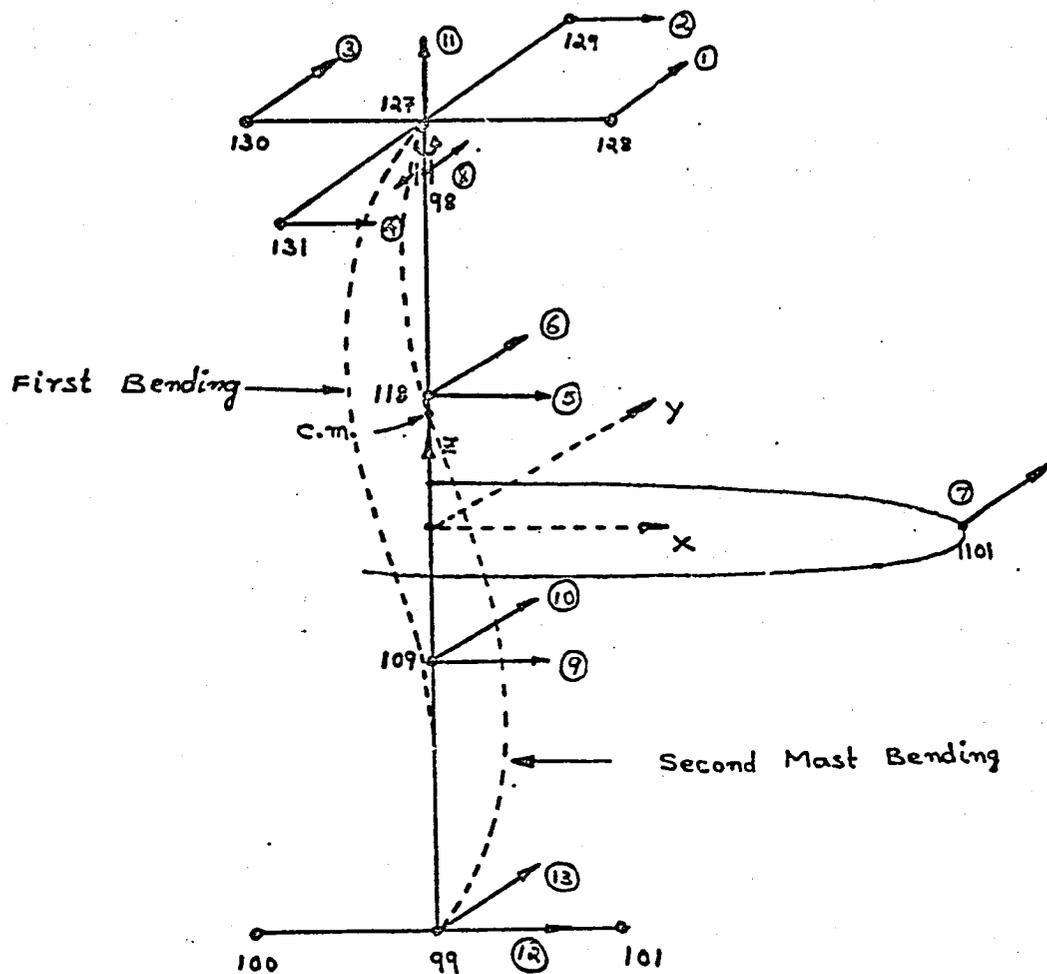
Actuator no.	Mode being affected
1 2 3 and 4	Feed Mast Torsion (12)
5	First Bending (about y axis) (8)
6	First Bending (about x axis) (9)
7	Surface Torsion (10)
8 (torquer)	Yaw (rotation about z axis) and First Torsion (7)
9	Translation along x } Also second
10	Translation along y } Mast bending
11	Translation along z
12	Pitch (rotation about y axis)
13	Roll (rotation about x axis)

Fig. 5.3 Proposed Arrangement of Actuators – Hoop/Column
Antenna System

Columns

- 2 -

① ② ③ ④ ⑤ ⑥ ⑦ ⑧ ⑨ ⑩ ⑪ ⑫ ⑬

Rows 128 $\begin{bmatrix} 0 \\ 1 \\ 0 \\ 0 \\ 0 \\ 0 \end{bmatrix}$ B(128,2,1)
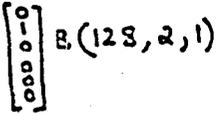
129 $\begin{bmatrix} 1 \\ 0 \\ 0 \\ 0 \\ 0 \\ 0 \end{bmatrix}$ B(129,1,2)

130 $\begin{bmatrix} 0 \\ 1 \\ 0 \\ 0 \\ 0 \\ 0 \end{bmatrix}$ B(130,2,3)

131 B(131,1,4) $\begin{bmatrix} 1 \\ 0 \\ 0 \\ 0 \\ 0 \\ 0 \end{bmatrix}$

118 B(118,1,5) $\begin{bmatrix} 1 \\ 0 \\ 0 \\ 0 \\ 0 \\ 0 \end{bmatrix}$ $\begin{bmatrix} 0 \\ 1 \\ 0 \\ 0 \\ 0 \\ 0 \end{bmatrix}$ B(118,2,6)

1101 B(1101,2,7) $\begin{bmatrix} 0 \\ 1 \\ 0 \\ 0 \\ 0 \\ 0 \end{bmatrix}$

98 B(98,6,8) $\begin{bmatrix} 0 \\ 0 \\ 0 \\ 0 \\ 0 \\ 1 \end{bmatrix}$

109 B(109,1,9) $\begin{bmatrix} 1 \\ 0 \\ 0 \\ 0 \\ 0 \\ 0 \end{bmatrix}$ $\begin{bmatrix} 0 \\ 1 \\ 0 \\ 0 \\ 0 \\ 0 \end{bmatrix}$ B(109,2,10)

127 B(127,3,11) $\begin{bmatrix} 0 \\ 0 \\ 1 \\ 0 \\ 0 \\ 0 \end{bmatrix}$

99 B(99,1,12) $\begin{bmatrix} 1 \\ 0 \\ 0 \\ 0 \\ 0 \\ 0 \end{bmatrix}$ B(99,2,13) $\begin{bmatrix} 0 \\ 1 \\ 0 \\ 0 \\ 0 \\ 0 \end{bmatrix}$

5.4   Schematic of Control Influence Matrix with 13 Actuators

5.10
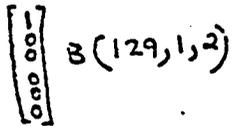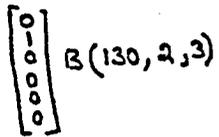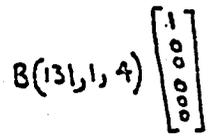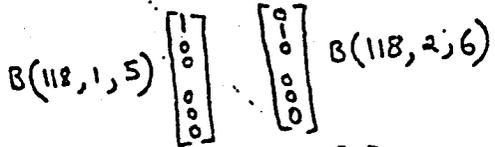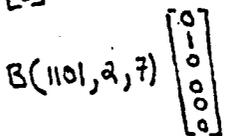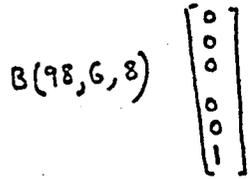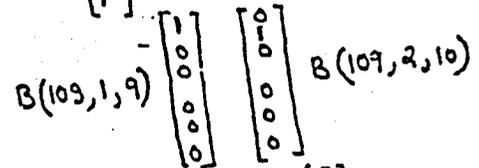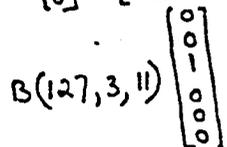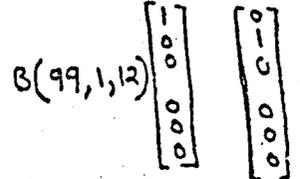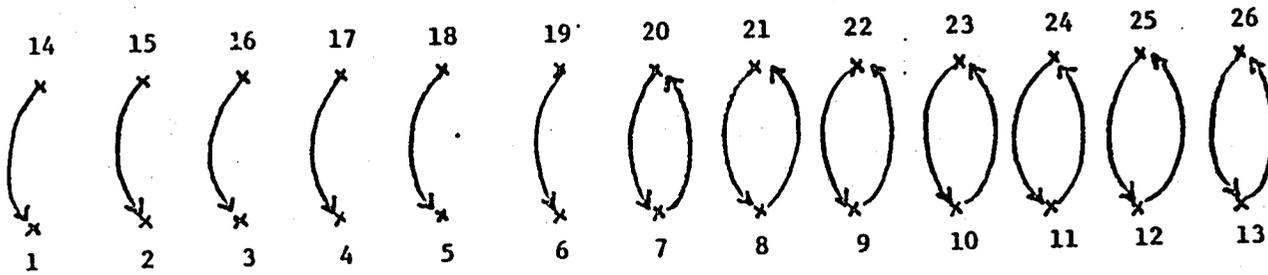
Fig. 5.5   Digraph of Matrix A   -   Hoop/Column with 13 Modes.

Actuator Number	Location	
	node	degree of freedom
1	128	2
2	129	1
3	130	2
4	131	1
5	118	1
6	118	2
7	1101	2
8	98	6
9	109	1
10	109	2
11	127	3
12	99	1
13	99	2

Table 5.1 Location of Actuators.

128,2	129,1	130,2	131,1	118,1	118,2	101,2
0.449843D-12	-0.756900D-13	-0.290445D-12	-0.517727D-12	0.635040D 00	0.648747D-14	0.0
0.101490D-11	-0.106732D-11	0.111974D-11	0.107778D-11	0.352945D 00	0.302576D-13	0.0
0.532660D 00	0.500000D 00	-0.467341D 00	-0.500000D 00	0.188515D-12	0.500000D 00	0.100000D 01
0.274500D 00	-0.285378D 00	0.296255D 00	0.285378D 00	-0.209589D-04	-0.146809D-01	0.333049D 00
0.426064D-01	-0.997478D-01	0.156889D 00	-0.997478D-01	0.118020D-05	-0.114991D 00	0.749611D 00
0.356486D 00	0.356832D 00	-0.357179D 00	-0.356832D 00	-0.135975D-04	-0.894211D-02	-0.259095D 00
0.308903D 01	0.121904D 00	0.333284D 01	-0.121904D 00	-0.278844D-10	0.208694D 00	0.100000D 01
0.392277D-11	0.191113D-11	0.100506D-12	-0.188884D-11	0.100000D 01	-0.567217D-11	-0.231955D-11
0.338250D-02	-0.523665D-01	0.101351D 00	0.523665D-01	-0.992926D-10	-0.100000D 01	0.226015D 00
0.219473D-03	0.129115D-04	-0.245696D-03	-0.129115D-04	-0.317243D-12	-0.679824D-04	-0.728512D-01
0.247914D-01	-0.208447D-01	0.168979D-01	0.208447D-01	0.691887D-10	-0.390973D-01	-0.303313D-02
0.747262D-01	-0.479013D-02	0.843065D-01	0.479013D-02	0.726125D-11	-0.446188D-01	0.100000D 01
0.615937D-10	0.492684D-10	-0.369430D-10	-0.492502D-10	0.487755D 00	-0.654727D-09	-0.160330D-09

98,6	109,1	109,2	127,3	99,1	99,2
0.451683D-15	0.277117D 00	0.282408D-12	-0.362893D-12	0.0	-0.276528D-12
0.293694D-15	0.717990D 00	0.682283D-12	-0.315554D-12	0.100000D 01	-0.334105D-12
0.204442D-03	0.747177D-12	0.500000D 00	-0.369926D-12	0.102108D-11	0.500000D 00
0.682555D-04	-0.865246D-03	0.251979D 00	-0.500000D 00	-0.151745D-02	0.457972D 00
0.358566D-03	0.487220D-04	-0.130006D 00	-0.281550D-01	0.854479D-04	-0.141606D 00
0.217342D-05	-0.561343D-03	0.369262D 00	0.324383D 00	-0.984474D-03	-0.647607D 00
0.179886D-01	-0.506974D-10	0.388303D-01	0.493154D-13	-0.435442D-10	-0.354616D-01
0.159190D-13	0.146673D 00	-0.229063D-11	-0.965277D-02	-0.921111D-01	-0.193719D-11
0.275832D-03	-0.249343D-09	0.163547D 00	0.107042D-12	0.217673D-09	-0.677794D-01
0.134647D-05	-0.647414D-13	-0.126562D-04	0.516825D-14	-0.183262D-14	0.311753D-05
0.228238D-04	0.228926D-09	0.548173D 00	0.129680D-12	-0.199225D-09	-0.419767D-01
0.247478D-02	0.201241D-10	0.980488D-03	-0.407813D-13	-0.207007D-10	-0.716639D-03
0.123786D-12	0.406908D 00	-0.925288D-10	0.105982D-02	-0.725563D-01	0.108981D-10

Table 5.2 $\phi^T B$ for 13 Actuators

VI. DEVELOPMENT OF ALGORITHM TO EVALUATE HOOP/COLUMN COUPLING COEFFICIENTS

The generic mode equations and the equations of rotational motion of
a flexible orbiting body contain coupling terms between the rigid and flexi-
ble modes and terms due to the coupling within the flexible modes that are
assumed to be small and, thus, are usually neglected when a finite element
analysis of the dynamics of the system is undertaken. In this Chapter
a computational algorithm that permits the evaluation of the coefficients
in these coupling terms in the equations of motion as applied to a finite
element model of the Hoop/Column system is developed.

Using a Newton-Euler approach, one-can express the equations of motion
of an elemental mass of the system, in the frame moving with the body, as[1]

$$\{\bar{a}_{cm} + \ddot{\bar{r}} + 2\bar{\omega} + \dot{\bar{r}} + \dot{\bar{\omega}}x\bar{r} + \bar{\omega}x(\bar{\omega}x\bar{r})\}\rho dv = \{\bar{f} + \bar{e} + L(\bar{q})/\rho\}\rho dv \qquad (6.1)$$

where ρ = mass per unit volume,

$\bar{e}$ = external forces per unit mass,

$\bar{q}$ = elastic transverse displacements of the
element of volume.

$\bar{f}$ = force due to the gravity on the unit mass, and

L = the linear operator which when applied to $\bar{q}$ yields
the elastic forces acting on the element of volume
considered.

$\bar{r}$ = position vector of element dv

$\bar{\omega}$ = inertial angular velocity of the body frame

VI.1 EQUATIONS OF ROTATIONAL MOTION

The equations of rotational motion of the body are obtained by taking
the moments of all the external, internal and inertial forces acting on
the body, i.e., from Eq. (6.1)

$$\int \bar{r} \times [\bar{a}_{cm} + \ddot{\bar{r}} + 2\bar{\omega}\times\dot{\bar{r}} + \dot{\bar{\omega}}\times\bar{r} + \bar{\omega}\times(\bar{\omega}\times\bar{r})]\rho dv$$

$$= \int_v \bar{r}\times[L(\bar{q})/\rho + \bar{f} + \bar{e}]\rho dv \qquad (6.2)$$

one can obtain the following form for the equations of rotational
motion.

$$\bar{R} + \sum_{n=1}^{\infty} \bar{Q}^{(n)} + \sum_{n=1}^{\infty} \bar{D}^{(n)} = \bar{G}_R + \sum_{n=1}^{\infty} \bar{G}^{(n)} + \bar{C} \qquad (6.3)$$

where $\bar{R} = \int_v [\bar{r}_o\times(\dot{\bar{\omega}}\times\bar{r}_o) - (\bar{r}_o\cdot\bar{\omega})(\bar{\omega}\times\bar{r}_o)]\rho dv$

$$\sum_{n=1}^{\infty} \bar{Q}^{(n)} = \int_v [\bar{r}_o\times\ddot{\bar{q}}+2\bar{r}_o\times(\bar{\omega}\times\dot{\bar{q}})+\bar{r}_o\times(\dot{\bar{\omega}}\times\bar{q})+\bar{q}\times(\dot{\bar{\omega}}\times\bar{r}_o)$$

$$-(\bar{r}_o\cdot\bar{\omega})(\bar{\omega}\times\bar{q})-(\bar{q}\cdot\bar{\omega})(\bar{\omega}\times\bar{r}_o)]\rho dv$$

$$\sum_{n=1}^{\infty} \bar{D}^{(n)} = \int_v \bar{q}\,\rho dv\times(\bar{a}_{cm}-\bar{f}_o) + \sum_{n=1}^{\infty} \omega_n^2 A_n \int_v \bar{r}_o\times\bar{\phi}^{(n)}\rho dv$$

$$\bar{G}_R = \int \bar{r}_o\times M\bar{r}_o\,\rho dv$$

$$\sum_{n=1}^{\infty} \bar{G}^{(n)} = \int_v [\bar{r}_o\times M\bar{q}+\bar{q}\times M\bar{r}_o]\rho dv$$

$$\bar{C} = \int_v \bar{r}\times\bar{e}\,\rho dv$$

$$\bar{r} = \bar{r}_o + \bar{q}$$

M = matrix operator[1] which when applied to $\bar{r}$ yields gravity-gradient forces

$\bar{a}_{cm}$ = acceleration of the center of mass

$\bar{f}_o$ = force/mass due to gravity at the undeformed center of mass

$\bar{\phi}^{(n)}$ = modal shape vector for the nth mode

ω_n = frequency of the nth mode

A_n = time dependent modal amplitude function

VI. 2 GENERIC MODE EQUATIONS

The generic mode equation is obtained by taking the modal components of all internal, external and inertial forces acting on the body, i.e.,

$$\int_v \bar{\phi}^{(n)} \cdot [\bar{a}_{cm} + \ddot{\bar{r}} + 2\bar{\omega} x \dot{\bar{r}} + \dot{\bar{\omega}} x \bar{r} + \bar{\omega} x (\bar{\omega} x \bar{r})] \, \rho dv$$

$$= \int_v \bar{\phi}^{(n)} \cdot [L(\bar{q})/\rho) + \bar{f} + \bar{e}] \, \rho dv \tag{6.4}$$

The generic mode equation is obtained in the following form:

$$\ddot{A}_n + \omega_n^2 A_n + \mathcal{G}_n/M_n + \sum_{m=1}^{\infty} \mathcal{G}_{mn}/M_n = [g_n + \sum_{m=1}^{\infty} g_{mn} + E_n + D_n']/M_n \tag{6.5}$$

where $\mathcal{G}_n = \int_v [\bar{\phi}^{(n)} \cdot \dot{\bar{\omega}} x \bar{r}_o + \bar{\phi}^{(n)} \cdot \bar{\omega} x (\bar{\omega} x \bar{r}_o)] \rho dv$

$$\sum_{m=1}^{\infty} \mathcal{G}_{mn} = \int_v [2\bar{\phi}^{(n)} \cdot \bar{\omega} x \dot{\bar{q}} + \bar{\phi}^{(n)} \cdot \dot{\bar{\omega}} x \bar{q} + \bar{\phi}^{(n)} \cdot \bar{\omega} x (\bar{\omega} x \bar{q})] \, \rho dv$$

$$g_n = \int \bar{\phi}^{(n)} \cdot \bar{M} \bar{r}_o \rho dv ; \quad \sum_{m=1}^{\infty} g_{mn} = \int_v \bar{\phi}^{(n)} \cdot \bar{M} \bar{q} \rho dv ;$$

$$E_n = \int \bar{\phi}^{(n)} \cdot \bar{e} \rho dv \text{ and } D_n' = \int_v \bar{\phi}^{(n)} \rho dv \cdot (\bar{a}_{cm} - \bar{f}_o).$$

VI.3 CARTESIAN COMPONENTS OF THE DIFFERENT COUPLING TERMS

The expressions for $\bar{R}$, $\bar{Q}^{(n)}$, $\bar{G}_R$, $\bar{G}^{(n)}$, $\mathscr{G}_n$, $\mathscr{G}_{mn}$, g_n, g_{mn} in Cartesian components are presented in this section.

One can express the following vectors in their Cartesian component form as

$$\bar{r}_o = \xi_x \hat{i} + \xi_y \hat{j} + \xi_z \hat{k}; \quad \bar{\omega} = \omega_x \hat{i} + \omega_y \hat{j} + \omega_z \hat{k}$$

$$\bar{q} = \sum_{n=1}^{\infty} A_n(t) \bar{\phi}^{(n)}(\bar{r}_o); \quad \bar{\phi}^{(n)} = \phi_x^{(n)} \hat{i} + \phi_y^{(n)} \hat{j} + \phi_z^{(n)} \hat{k}$$

$$\bar{Q}^{(n)} = Q_x^{(n)} \hat{i} + Q_y^{(n)} \hat{j} + Q_z^{(n)} \hat{k}$$

and
$$\bar{G}^{(n)} = G_x^{(n)} \hat{i} + G_y^{(n)} \hat{j} + G_z^{(n)} \hat{k},$$

where $\hat{i}$, $\hat{j}$, $\hat{k}$ are unit vectors along the body principal axes of inertia in the undeformed state; ξ_x, ξ_y, ξ_z are the co-ordinates of a point in the undeformed state.

With the use of the component forms of the vectors given above, one can expand the various vector expressions given in Eqs. (6.3) and (6.5) to obtain

$$\bar{R} = [J_x \dot{\omega}_x + (J_z - J_y) \omega_y \omega_z] \hat{i}$$
$$+ [J_y \dot{\omega}_y + (J_x - J_z) \omega_z \omega_x] \hat{j}$$
$$+ [J_z \dot{\omega}_z + (J_y - J_x) \omega_x \omega_y] \hat{k} \qquad (6.6)$$

$$Q_x^{(n)} = \ddot{A}_n (H_{yz}^{(n)} - H_{zy}^{(n)}) + 2\dot{A}_n [(H_{yy}^{(n)} + H_{zz}^{(n)}) \omega_x - H_{yx}^{(n)} \omega_y$$

$$- H_{zx}^{(n)} \omega_z] + A_n [2(H_{yy}^{(n)} + H_{zz}^{(n)}) \dot{\omega}_x - (H_{xy}^{(n)} + H_{yx}^{(n)}) \dot{\omega}_y$$

$$- (H_{zx}^{(n)} + H_{xz}^{(n)}) \dot{\omega}_z - 2\omega_y \omega_z (H_{zz}^{(n)} - H_{yy}^{(n)}) - \omega_x \omega_y (H_{xz}^{(n)}$$

$$+ H_{zx}^{(n)}) + \omega_x \omega_z (H_{xy}^{(n)} + H_{yx}^{(n)}) + (\omega_z^2 - \omega_y^2)(H_{yz}^{(n)}$$

$$+ H_{zy}^{(n)})] \tag{6.7}$$

$$\bar{G}_R = (J_z - J_y) M_{23} \hat{i} + (J_x - J_z) M_{31} \hat{j} + (J_y - J_x) M_{21} \hat{k} \tag{6.8}$$

$$G_x^{(n)} = A_n [(M_{33} - M_{22})(H_{yz}^{(n)} + H_{zy}^{(n)}) - M_{21}(H_{xz}^{(n)} + H_{zx}^{(n)})$$

$$+ M_{31}(H_{xy}^{(n)} + H_{yx}^{(n)}) + 2M_{23}(H_{yy}^{(n)} - H_{zz}^{(n)})] \tag{6.9}$$

$$\mathcal{P}_n = \dot{\omega}_x (H_{yz}^{(n)} - H_{zy}^{(n)}) + \dot{\omega}_y (H_{zx}^{(n)} - H_{xz}^{(n)}) + \dot{\omega}_z (H_{xy}^{(n)} - H_{yx}^{(n)})$$

$$+ \omega_x \omega_y (H_{xy}^{(n)} + H_{yx}^{(n)}) + \omega_y \omega_z (H_{yz}^{(n)} + H_{zy}^{(n)}) + \omega_z \omega_x (H_{zx}^{(n)}$$

$$+ H_{xz}^{(n)}) - \omega_x^2 (H_{yy}^{(n)} + H_{zz}^{(n)}) - \omega_y^2 (H_{zz}^{(n)} + H_{xx}^{(n)})$$

$$- \omega_z^2 (H_{xx}^{(n)} + H_{yy}^{(n)}) \tag{6.10}$$

$$\mathcal{P}_{mn} = 2\dot{A}_m [\omega_x (L_{yz}^{(mn)} - L_{zy}^{(mn)}) + \omega_y (L_{zx}^{(mn)} - L_{xz}^{(mn)})$$

$$+ \omega_z (L_{xy}^{(mn)} - L_{yx}^{(mn)})] + A_m [\dot{\omega}_x (L_{yz}^{(mn)} - L_{zy}^{(mn)})$$

$$+ \dot{\omega}_y (L_{zx}^{(mn)} - L_{xz}^{(mn)}) + \dot{\omega}_z (L_{xy}^{(mn)} - L_{yx}^{(mn)})$$

$$+ \omega_x \omega_y (L_{xy}^{(mn)} + L_{yx}^{(mn)}) + \omega_y \omega_z (L_{yz}^{(mn)} + L_{zy}^{(mn)})$$

$$+ \omega_z \omega_x (L_{zx}^{(mn)} + L_{xz}^{(mn)}) - \omega_x^2 (L_{yy}^{(mn)} + L_{zz}^{(mn)})$$

$$- \omega_y^2 (L_{zz}^{(mn)} + L_{xx}^{(mn)}) - \omega_z^2 (L_{xx}^{(mn)} + L_{yy}^{(mn)})] \qquad (6.11)$$

$$g_n = \sum_{\alpha\beta} H_{\alpha\beta}^{(n)} M_{\alpha\beta}$$

$$g_{mn} = A_m \sum_{\alpha\beta} L_{\alpha\beta}^{(mn)} M_{\alpha\beta}$$

where $H_{\alpha\beta}^{(n)} = \int_V \xi_\alpha \phi_\beta^{(n)} dm$; $L_{\alpha\beta}^{(mn)} = \int_V \phi_\alpha^{(m)} \phi_\beta^{(n)} dm$; and $\alpha, \beta = x, y, z$ or $1, 2, 3$. When α is x in $H_{\alpha\beta}^{(n)}$ or $L_{\alpha\beta}^{(mn)}$ the corresponding value of α in $M_{\alpha\beta}$ is 1. In a similar way when α is y in $H_{\alpha\beta}^{(n)}$ or $L_{\alpha\beta}^{(mn)}$, α is 2 in $M_{\alpha\beta}$ and when α is z in $H_{\alpha\beta}^{(n)}$ or $L_{\alpha\beta}^{(mn)}$, α is 3 in $M_{\alpha\beta}$. The same reasoning holds for β also.

The expressions for $Q_y^{(n)}$ and $Q_z^{(n)}$ are obtained by the cyclic permutation of x, y, z in the expression for $Q_x^{(n)}$ in Eq. (6.7) and the expressions for $G_y^{(n)}$ and $G_z^{(n)}$ are obtained by the cyclic permutation of x, y, z in the expression for $G_x^{(n)}$ in Eq. (6.9).

For a discretized model the expressions for the volume integrals are replaced by the following summations:

$$H_{\alpha\beta}^{(n)} = \sum_{i=1}^{k} (\xi_\alpha)_i \, (\phi_\beta^{(n)})_i m_i \qquad (6.12)$$

$$(\alpha,\beta = x,y,z)$$

$$L_{\alpha\beta}^{(mn)} = \sum_{i=1}^{k} (\phi_\alpha^{(m)})_i \, (\phi_\beta^{(n)})_i m_i \qquad (6.13)$$

where

k = total number of discrete masses

i = index identifying a nodal point

m_i = mass concentrated at the ith node.

ξ_α = coordinates of m_i in the undeformed state

VI.4 EVALUATION OF COUPLING COEFFICIENTS IN THE EQUATIONS OF MOTION AS
APPLIED TO A FINITE ELEMENT MODEL OF THE HOOP/COLUMN SYSTEM

VI. 4.1 Model Description

The structural dynamic modeling of the Hoop/Column antenna has gone
through many stages before reaching the single surface model which will
be analyzed in this chapter.

Initially, it had 231 nodes distributed as follows: 192 nodes on
the 8 support circles including the hoop (24 nodes on each circle spaced
at 15° intervals); 28 nodes on the mast and the feed mast; and 11 nodes
at the points of location of the solar panels (upper and lower), the
S band reflector, and the feed panels (up-link and down-link)—see Figs.
5.1 and 5.2. After reduction the number of nodes was diminished to 114
including a total of 96 nodes on the circles: 1100, 1200, 1300, and 1400;
7 nodes on the mast and the feed mast; and 11 nodes at the locations of
the solar panels, the S band reflector, and the feed panels (Fig. 6.1).

VI. 4.2 Approximate Mass Distribution

From an unpublished document prepared by the Harris Corporation,[2] and submitted by NASA Langley Research Center, it has been possible to arrive at the mass distribution shown in Table 6.1. 9803.0 lb. out of the total weight of the Hoop/Column Antenna (10,070 lb.) were distributed between the final grid points. The distribution was done in agreement with the information found in the Harris Corporation document. The page numbers appearing in Table 6.1 refer to particular mass/moment of inertia calculations in the Harris Corporation document.[2]

The small (2%) discrepancy between the calculated total mass (9803.0 lb.) and the stated weight of the system (10,070 lb) is thought to be attributed to: (1) uncertainties in the weight of specific stringers; (2) uncertainties inherent with the finite element reduction technique where the initial mass must be redistributed between a reduced, final number of grid (node) points; and (3) other miscellaneous uncertainties, such as the exact weight/location of the optical instrument, etc.

VI. 4.3 Cartesian Coordinates of all the Nodal Points in the Final NASTRAN Output

Reference 2 contains the cylindrical coordinates of all the nodal points on the mast, the feed mast, and at the location of the panels and electronics. It also contains the Z coordinates of the planes which contain the circles along with their respective diameters. Thus, the Cartesian coordinates of all the nodal points were obtained by a simple transformation from cylindrical to Cartesian coordinates.

VI.4.4 Development of a Computational Algorithm for Evaluation of the Coupling Coefficients

After receipt of the tape containing the modal functions, this information was stored in our IBM 360 in such a manner that when one calls subroutine, GETMP(2), he can refer to the kth component of the Ith mode shape vector at the grid point J by VECMP(I,J,K). Based on this, an algorithm described in the flow diagram, Fig. 6.2, was designed and tested. As indicated in Fig. 6.2, the available data, such as: the Cartesian coordinates of the grid points on the mast, the feed mast and the ones at the locations on the appendages; and such as the mass concentrations at all the nodal points are input into the software routine and these data will consequently have to be updated according to any development in the Hoop/Column modeling. The subroutine, DCS, (given the radius of the circles and the Z component of their centers) computes the Cartesian coordinates of the nodal points on the circles.

Subroutine GETMP(2), which makes the $\phi_{J,k}^{(I)}$ available, is called and the values of components of the desired mode shape vector at the particular grid point are incorporated into a loop mathematically described by Eqs. (6.12) and (6.13). It should be noted that, for reasons of effectiveness, each coefficient is evaluated separately on the circles and on the other grid points and then combined to yield the corresponding coupling coefficient for the entire Hoop/Column system.

The algorithm has been tested for two modes (the 7th and the 8th) successfully, but only after the evaluation of the coefficients corresponding to all the 13 modes will one be able to make positive conclusions.

6.10

References - Chapter VI

1. Bainum, P.M., Kumar, V.K., and James, P.K., "The Dynamics and Control
    of Large Flexible Space Structures," NASA Report CR-156976, May 1978.

2. "Versatile Hoop/Column Antenna Structural Dynamic Model," unpublished
    document, Harris Corp, submitted by NASA Langley Research Center, (also
    including NASTRAN printout).

Indicates grid point where mode shape not printed out.
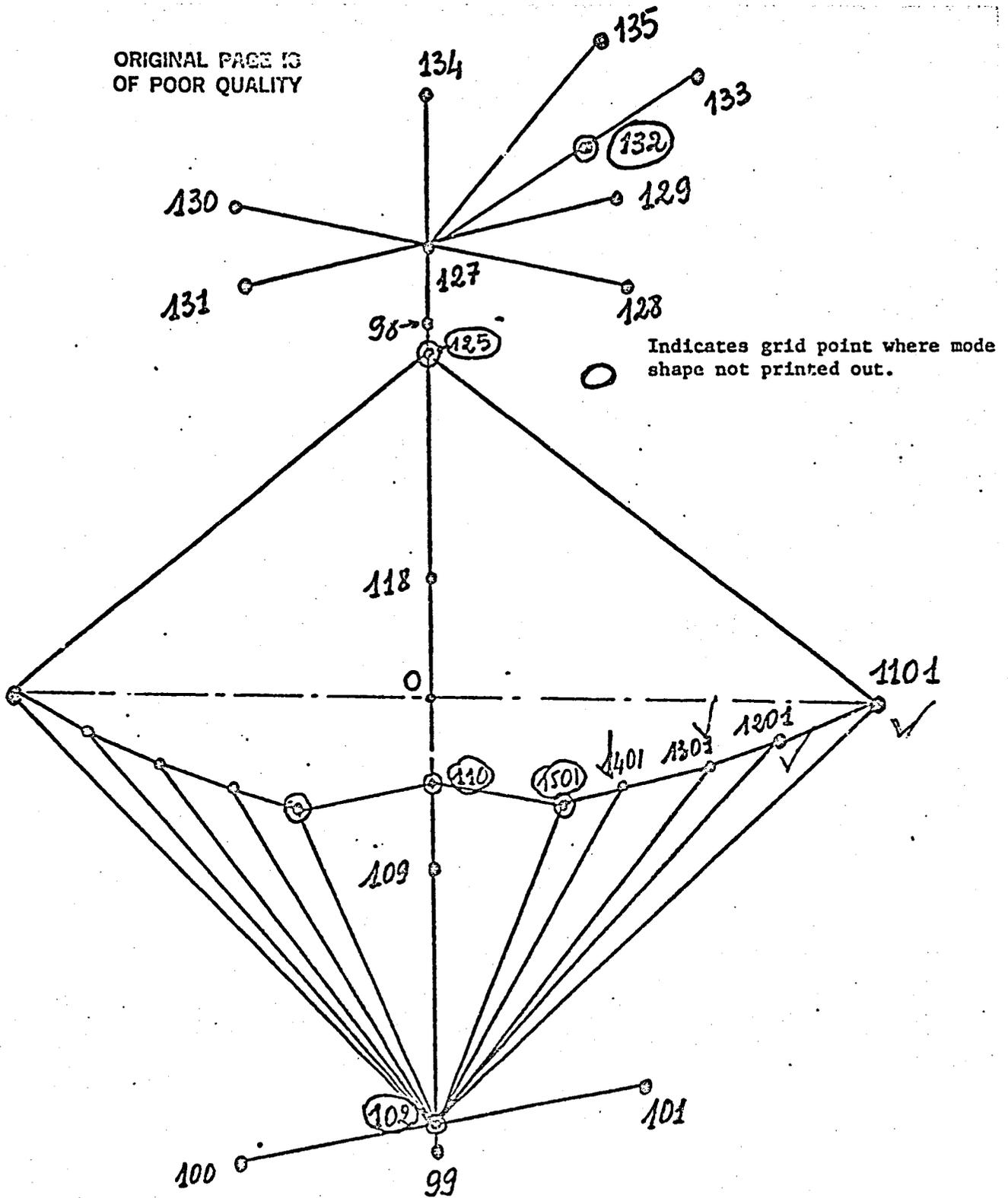
Fig. 6.1   Geometry of Single Surface Hoop/Column
            FEM Model.

Given X,Y,Z (cartesian coordinates of the nodal points on the mast and feed) and the mass concentration at each nodal point in the system (approximate mass distribution)

Call Subroutine DCS which computes X,Y, and Z of the nodal points on the different circles

Subroutine GETMP (2) makes $\phi_{J,K}^{(I)}$ available

I = mode number
J = node number
K = x,y,z component of $\vec{\phi}$

Feed + Mast Appendages

Circles

$$H_{\alpha\beta}^{(I)} = \sum_J \xi_\alpha \phi_{J,\beta}^{(I)} M_J$$

$$L_{\alpha\beta}^{mn} = \sum_I \phi_{J,\alpha}^m \phi_{j\beta}^n M_J$$

$$H_{\alpha\beta}^{(I)} = \sum_j \xi_\alpha \phi_{j,\beta}^{(I)} M_j$$

$$L_{\alpha\beta}^{mn} = \sum_j \phi_{j,\alpha}^m \phi_{j,\beta}^n M_j$$

For the total system
$$H_{\alpha\beta}^{(I)} \qquad L_{\alpha\beta}^{mn}$$

Fig. 6.2. Flow Diagram Describing the Algorithm Used in the Evaluation of the Coupling Coefficients.

| Grid points I.D. No.	Mast Assemb.	Feed Mast Page 77	Lower Solar Panels Page 85	Upper Solar Parel Page 81	Feed Panels Page 82	S band Feed Page 86	S band Reflector Page 82	Lower Electronics Page 84	Upper Electronics Page 84	Hoop Assemb. + Mesh +Reflector	Sub. Total at grid points in lbs.
98	320.00	30.00									350.00
99	320.00							1953.00			2273.00
100			144.50								144.50
101			144.50								144.50
109	320.00										320.00
118	320.00										320.00
127		30.00		327.50					1898.00		2255.50
128					548.13						548.13
129					481.87						481.87
130					543.13						548.13
131					481.87						481.87
133						255.00					255.00
134							130.00				130.00
135				327.50							327.50
1100 series										1027.00	1027.00
1200 series										49.00	49.00
1300 series										49.00	49.00
1400 series										49.00	49.00
1500 series										49.00	49.00

* Hoop assembly at grid points 1101, 1107, 1113, 1119; 244.51bs/point

TOTAL 9803.0

Table 6.1 Approximate Mass Distribution at Final Grid Points (Pounds)

VII. GENERAL CONCLUSIONS AND RECOMMENDATIONS

The widespread use of various computer algorithms required at different stages for the simulation of the dynamics and control of large flexible orbiting systems should be emphasized. Problem areas are mainly associated with the large order required to model such systems. The use of graph theoretic techniques can often be used to reduce the computational effort involved in the calculation of the eigenvalues of such large ordered systems. Computer generated interactive graphics can provide additional insight into the interpretation of the flexible modal shape functions of complex systems.

The graph theory approach can also be utilized to define controllability in terms of the term rank and input-state reachability concepts. This approach can be employed to examine the effects of inherent damping (usually expected to be present in LSST systems) on the number and locations of the required actuators. It is seen that the damping matrix does not influence the required number of actuators but offers greater flexibility to the possible locations of the actuators for which the system is controllable. The system (stiffness) matrix term rank deficiency dictates the number of actuators required and also influences the location of the actuators.

A mathematical model of the solar radiation forces and moments acting on a free-free flexible beam in orbit has been developed. For small pitch angles, it is seen that the solar radiation torques due to the deformations of the beam can be larger than those due to the gravity-gradient for orbits near synchronous altitude.

In-orbit-plane steady state open-loop (uncontrolled) responses for different initial beam deflections indicate that, in general, the effects of solar pressure on the modal amplitudes are small, but the magnitude of the induced pitch oscillations can be relatively larger. Future work could extend the model to plate and shell surfaces, and also assess the effect of the solar pressure disturbance on previously developed control laws, designed primarily to provide certain transient response characteristics.

A preliminary analysis of the finite element dynamic model using the first 13 modes of the 122m. Hoop/Column antenna system indicates that a minimum of six properly placed actuators is required for controllability. Additional work is currently underway to analyze transient responses and force-impulse requirements for control laws based on different techniques using ORACLS, and also various combinations of number and location of actuators.

Finally, an algorithm has been developed to evaluate the various coupling terms between the rigid rotational and flexible modes and also the intra-modal coupling terms in the equations of motion using the Hoop/Column mass distribution as provided by the NASTRAN finite element program as an example. Such coupling terms are usually not included in finite element models which are based on the earth-based vibrational and rigid modes only. Current work is in progress to evaluate the order of magnitudes of these terms – at least for the first 13 modes that are being used in Hoop/Column controls analysis.

END

DATE

FILMED

DEC 9 1982